University of Padova

Department of Industrial Engineering

Aerospace Engineering Master

Performance analysis of a multi-plate thermal control system for space and planetary probes

Laboratory test and stratospheric flight results of the POLARIS experiment

Graduand

Riccardo Dalla Vecchia

Supervisor

Prof. Alessandro Francesconi

Academic Year 2014 - 2015

Dedicated to my parents, who gave me a chance to prove and improve through all my walks of life. Please do not ever change

The first step is to establish that something is possible; then probability will occur.

Elon Musk

Contents

1 Thermal control of Spacecrafts **1**

1.1 Space environment 1

1.2 Thermal Control System 4

1.3 Space radiators 6

1.4 State of the art 10

2 Multi plate radiator **15**

2.1 POLARIS Experiment 15

2.2 Theoretical background 21

2.3 Thermal simulation 26

3 Laboratory test **29**

3.1 Testing setup 29

3.2 Test results 35

4 Stratospheric flight **41**

4.1 Flight data 41

4.1.1 Pressure and altitude 42

4.1.2 Environment temperatures 43

4.1.3 Incoming Radiation 45

4.2 Experiment behavior in stratosphere 48

5 Performance Analysis **53**

5.1 Flight analysis 54
5.2 Test analysis 60
5.3 Performance of the setup 63

6 Conclusions **67**

Bibliography **72**

Glossary **73**

List of Figures

1.1 The International Space Station, radiators in white. Credits NASA 2
1.2 Solar Radiation Spectrum[7] 3
1.3 Example of venetian style louvers 7
1.4 Theoretical effective emittance versus number of layers 9
1.5 Picture of the Rosetta thermal louvers. Copyright ESA-A. Le Floc'h 11
1.6 Picture of the MPO radiator. Credit: ESA 12
1.7 Drawing of the MESSENGER probe. Credit: NASA 13

2.1 Drawing of the experiment setup 16
2.2 Detail of the actuation mechanism 17
2.3 Focus on the experiment parts 19
2.4 Picture of the experiment setup 20
2.5 Schematic of the multi plate configuration 22
2.6 Example of thermal simulation 26
2.7 Example of thermal simulation (whole BEXUS flight) 27
2.8 Temperature distribution over radiator plates, simulated . . . 28

3.1 The experiment power supply and the notebook running the ground-segment software during the test campaign in the CISAS vacuum chamber 30
3.2 The experiment in the vacuum chamber 32

3.3 Drawing of the RTDs and the DP disposition over the radiator plates . . . 33
3.4 Example of the software GUI of the experiment . . . 34
3.5 Example of raw temperature data from three different tests . . 36
3.6 Normalized temperature data from three different tests 37
3.7 Average temperature values . . . 38
3.8 Temperature gradient over the radiator plates . . . 39
3.9 Incoming IR radiation . . . 40

4.1 Picture of the POLARIS experiment during the flight . . . 41
4.2 Pressure during the flight . . . 43
4.3 Altitude during the flight . . . 44
4.4 Ambient temperature during the flight . . . 45
4.5 Incoming visible and IR radiation during the flight . . . 46
4.6 Incoming visible radiation during the ascending phase . . . 46
4.7 Windows used for the FFT . . . 47
4.8 FFT results . . . 48
4.9 POLARIS vs a classic radiator . . . 50

5.1 POLARIS actuations during the stratospheric flight . . . 55
5.2 Direct heat fluxes applied to the radiator . . . 56
5.3 Heat flux within the radiator . . . 57
5.4 Heat flux within the radiator . . . 58
5.5 Average DP and external plate temperature values . . . 61
5.6 Average DP and external plate temperature values . . . 63
5.7 The net radiative flux exchanged between the external plate and the environment . . . 64
5.8 Picture of the experiment setup . . . 65

6.1 Detail of the different behavior between POLARIS and a standard radiator . . . 68
6.2 The POLARIS team . . . 70

Abstract

This work of thesis aims to study the performances of a new concept of heat radiator. This radiator is innovative because, contrary to the present ones, it is capable not only to vary the thermal resistance and, thus, the heat flux exchanged towards the environment, but to basically change the nature of the link between the payload and the surroundings, as will be better described in the following chapters.

All the data acquired are based on a test setup called POLARIS (POlimer-Actuated Radiator with Independent Surfaces).

This concept of radiator is intended to operate on planetary probes lacking an accurate attitude control and exposed to environmental changes; these conditions are close to those the experiment experienced during a stratosphere flight in October 2014 on a BEXUS balloon in the framework of the REXUS/BEXUS programme, which is realised under a bilateral Agency Agreement between the German Aerospace Center (DLR) and the Swedish National Space Board (SNSB). The Swedish share of the payload has been made available to students from other European countries through a collaboration with the European Space Agency (ESA).

Chapter 1

Thermal control of Spacecrafts

1.1 Space environment

All spacecrafts, artificial satellites and space stations have to exchange heat with the outer environment in order to keep serviceable all the on-board systems or to sustain an ambient temperature opportune to human living. In particular, a spacecraft in a low Earth orbit (LEO) receives electromagnetic radiation from three primary external sources. The most influential source is the direct solar flux. The average value of this solar flux at the mean Sun-Earth distance is called *solar constant*[1], which has been set as community's agreement at the value of 1366.1 W/m^2. The currently measured 1-sigma variation of the composite dataset of space based measurements is approximately 0.6 W/m^2 and there is a long-term (yearly) smoothed solar cycle minimum to maximum relative variation about the mean value of approximately 1.4 W/m^2, as is shown in table 1.1; therefore this is not really a constant but varies by about 3.4% during each year because of the slightly elliptical orbit of the Earth around the Sun[2].

[1]The solar constant varies geometrically with the Earth's distance from the sun and with the Sun's magnetic field activity on short to long timescales, as well as with the observer's heliocentric latitude

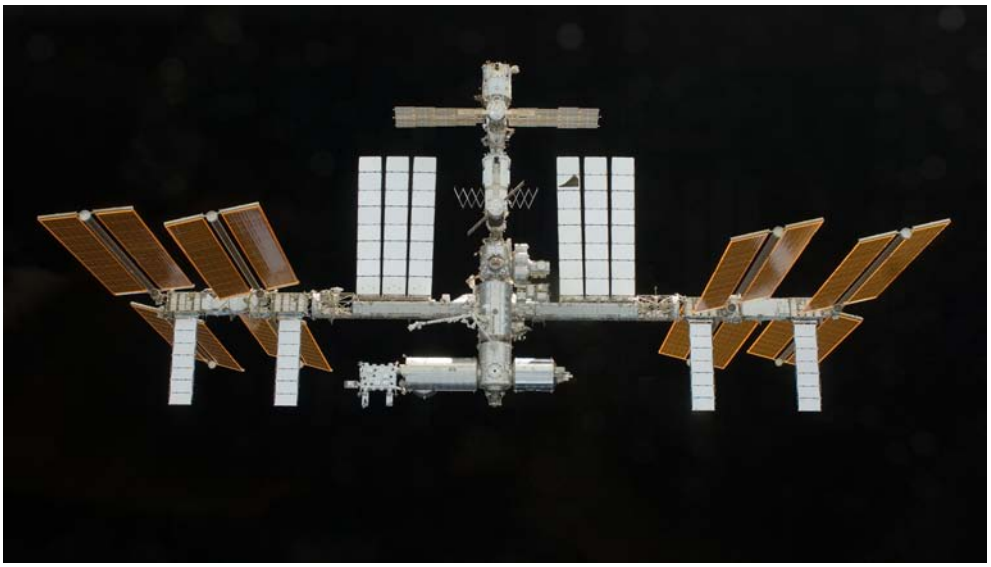

Figure 1.1: The International Space Station, radiators in white. Credits NASA

Table 1.1: Solar constant values

	W/m^2
Solar constant at 1 AU	1366.1
Solar energy flux at aphelion	1321.6
Solar energy flux at perihelion	1412.9

The two components of this radiation that we consider here are the visible, which comes from the solar photosphere (which is only about 400 km thick, has a temperature of approximately 5000 to 6000 K, and yet is responsible for the greatest percentage of the total solar radiation) in the range between 350 to 750 nm, and the infra-red (IR) in the range between 750 nm to 1 mm. In fact the solar spectrum shall be approximated by a black body curve with a characteristic temperature of 5762 K, as shown in figure 1.2. The effect of the other radiation, such as UV and X rays induce less influence on the Thermal Control System (TCS).

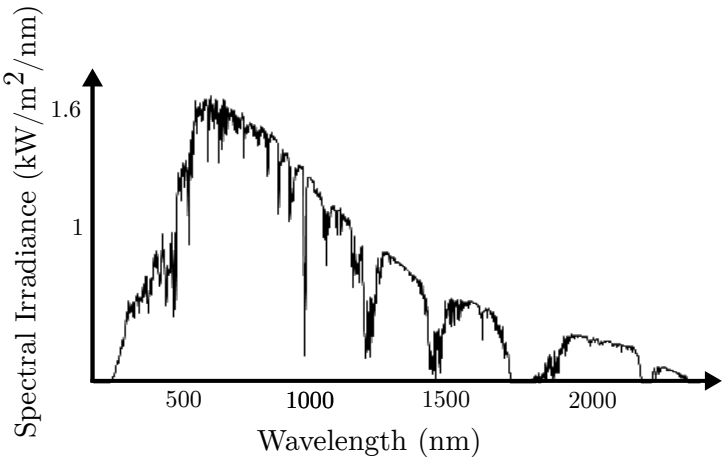

Figure 1.2: Solar Radiation Spectrum[7]

The two others radiation sources are the fraction of the incident sunlight reflected off the planet, termed albedo, and the planetary (Earth in this case) IR radiation.

Albedo is the fraction of sunlight which is reflected off a planet or moon and is only applicable when the portion of the planet that is seen by the spacecraft is sunlit. Usually it is expressed as a percentage of incident sunlight and is assumed to be diffuse. For the albedo the same spectral shape as for sunlight is assumed, but actual albedo spectrum can change, depending on properties of the surface (different materials can lead to absorption in certain wavelength bands and result in a highly variable spectrum) or of the atmosphere. An average value of the albedo constant of the planets in the solar system is reported in table 1.2. The variation of flux due to the albedo is not negligible, in fact, if any satellite component is sensitive to albedo loads and has a low thermal, mass may require that also albedo variation around the orbit be considered.

Planets not only reflect sunlight, they also emit low-wave IR radiation. Indeed, they achieves thermal equilibrium by balancing the energy received from the Sun with the energy re-emitted by themselves. The intensity of IR

energy emitted at a given time can vary considerably depending on factors such as surface and air temperature, atmospheric moisture content and cloud coverage. As with albedo, orbit average values are shown in table 1.2, but for spacecrafts with a particular sensitivity to variations in loads around the orbit more accurate analysis has to be done.

Table 1.2: Reference values for average planetary albedo and IR radiation [2]

Planet	Average Albedo	Average IR (K)
Mercury	0.106	442
Venus	0.65	231.7
Earth	0.3	288
Mars	0.15	210.1
Jupiter	0.52	110
Saturn	0.47	81.1
Uranus	0.51	58.2
Neptune	0.41	46.6

During a mission a spacecraft face many other heat sources, e.g. those present in the initial ascending phase, those due to the rocket propulsion or free molecular heating, but in this essay are neglected, in order to cover more accurately the TCS tasks during the operational phases of the spacecraft. Moreover, while TCS is comprehensive of many devices, such as different materials and surface finishes, insulation blankets, heaters and refrigerators, here we focus only on radiators.

1.2 Thermal Control System

In spacecraft design, the thermal control system (TCS) has the function to keep all the spacecraft parts within acceptable temperature ranges during all mission phases, avoiding failures due to freezing or overheating. It has

to withstand the external environment, which can vary in a wide range as described in section 1.1, and rejecting to space the internal heat dissipation of the spacecraft itself. This is required for two main reasons:

1. All the electronic and mechanical devices are design to operate in a narrow range of temperature; lifespan and reliability of those devices are related to the environmental conditions they face. Furthermore many different payloads may have more constricting temperature requirements.

2. Most materials used in aerospace industry have non-zero coefficients of thermal expansion and hence temperature changes imply thermal distortion: spacecrafts require high structural stability and therefore thermally induced distortion must be strictly controlled.

The temperature ranges required in order to work in an optimal efficiency state of the main components of a spacecraft are shown in table 1.3 [12]: those ranges derivate from the fact that most components are designed to efficiently work on Earth. Although electrical and mechanical devices used in military and aerospace applications must endure greater temperature range, usually between $-55°C$ and $125°C$, the operative thermal range is usually reduced to the minimum in order to achieve a superior reliability for the above mentioned components and a longer MTBF.

The TCS is usually composed by three different sub-systems. First of all, by devices interacting with the environment; either the surfaces need to be protected from the environment or there has to be improved interaction. Then devices dedicated to collect and transport heat. This includes the removal of dissipated heat from the equipment in which it is created to avoid unwanted increase in the spacecraft temperature and its carriage to the radiating devices. Eventually many spacecrafts has also devices dedicated to heat provisioning and storage, in order to precisely maintain a desired temperature (e.g. phase-change materials (PCM)).

Table 1.3: Components operative temperature ranges

	Min [$°C$]	Max [$°C$]
Electronic equipment	-15	50
Batteries	0	20
Mechanisms	0	50
IR detectors	-270	-170
Solar panels	-100	125

Thermal control is what allows maintaining the satellite's (or another space system) temperatures within set parameters during its lifetime. For instance, a piece of equipment could, if encountering a temperature level which is too high, be damaged or its performance could be severely affected. In space it would hardly be possible to correct such a problem and this is why space thermal control systems - like other space subsystems - need to be properly designed and tested and need to be very efficient and highly reliable. Thermal control is also what keeps the specified temperature stability for delicate electronics or optical components so as to ensure that they perform as efficiently as possible. ESA definition of thermal control

1.3 Space radiators

Ideally, thermal control of a satellite or component would be achieved using only passive techniques, such as surface finishes. Unfortunately, variation in environment conditions and internal heat generation, along with the degradation of the surface finishes over time, can drive temperature variations to ranges larger than some components can withstand. Therefore, since the beginning of the space exploration era many active devices have been developed and nowadays there are a lot of different technologies that are able to control the heat fluxes.

Radiators occur in several different forms, such as satellite structural panels, flat-plate radiators mounted to the side of the satellite, or panels that are deployed after the spacecraft orbit acquisition. Whatever the configuration, all radiators reject heat by IR radiation from their surfaces. The radiating power is dependent on the emittance of the surface and its temperature, following the formula 1.1.

$$Q = A \cdot \varepsilon \cdot \sigma \cdot T^4 \tag{1.1}$$

The radiator must reject both the satellite waste heat plus any radiant-heat load coming from the environment.

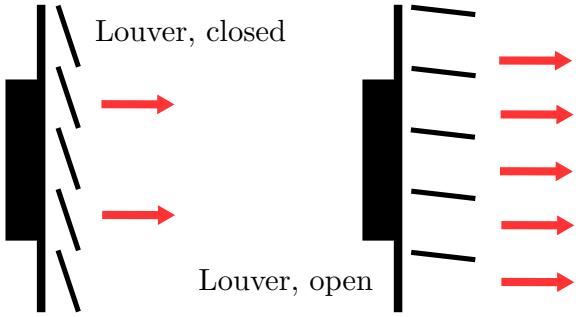

Figure 1.3: Example of venetian style louvers

Many solutions have been designed to overcome this problem. Most of them involve[5]:

Heaters these devices are sometimes required to protect components under cold-case environmental conditions or to make up for heat that is not dissipated when an electronic box is turned off. Heaters may also be used with thermostats or solid-state controllers to provide precise temperature control of a particular component. A third common use for heaters is to warm-up components to their minimum operating temperatures before they are turned on.

Louvers these are active elements that have been used in different forms on numerous spacecraft. In general, louvers can provide about six-to-one variation in heat rejection from fully closed to fully open without any power consumption. Thus, they find applications where the internal power dissipation varies rather widely due to duty-cyclic considerations. Louver assemblies can be very different, but the most used is the *venetian blind* type. This consist in a low-absorbance-to-emittance ratio baseplate covered by blades that give variable radiation characteristic to the baseplate. The blades are driven by the actuators that usually consist in bimetallic spirals or bellows.

Thermoelectric Coolers that use the Peltier effect[2], typically between two semiconductor (p-type and n-type) connected by a metallic conductor. These devices have been used for modest ($10 - 20^{\circ}$ C) local cooling applications and are reliable and compact, but are poorly efficient and ma have some structural problems due to different thermal coefficients of expansion of joined materials.

Phase-Change Materials normally used to maintain a target temperature for cyclically operating components that produce a large amount of heat in short time. PCM use a substance with a high heat of fusion which, melting and solidifying at a certain temperature, is capable of storing and releasing large amounts of energy. Heat is absorbed or released when the material changes from solid to liquid and vice versa. PCM systems are totally passive and very reliable, however they can show problems connected to the volume change of the device due to the phase change.

Pumped Fluid Loops are devices that provide efficient transfer of a large amount of thermal energy between two points by means of forced liquid

[2]The cooling of one junction and the heating of the other when electric current is maintained in a circuit of material consisting of two dissimilar conductors

convective cooling. The working fluid is recirculated by a pump within the system once its thermal energy has been radiated to space via a radiator. Those devices are usually very efficient but have problems related to the use of fluids and pumps.

It is also important to remember that in many scenario it is necessary not to waste heat and thus an insulation system is required; such systems are designed to minimize radiative exchanges and are normally referred to as Multi Layer Insulator (MLI).

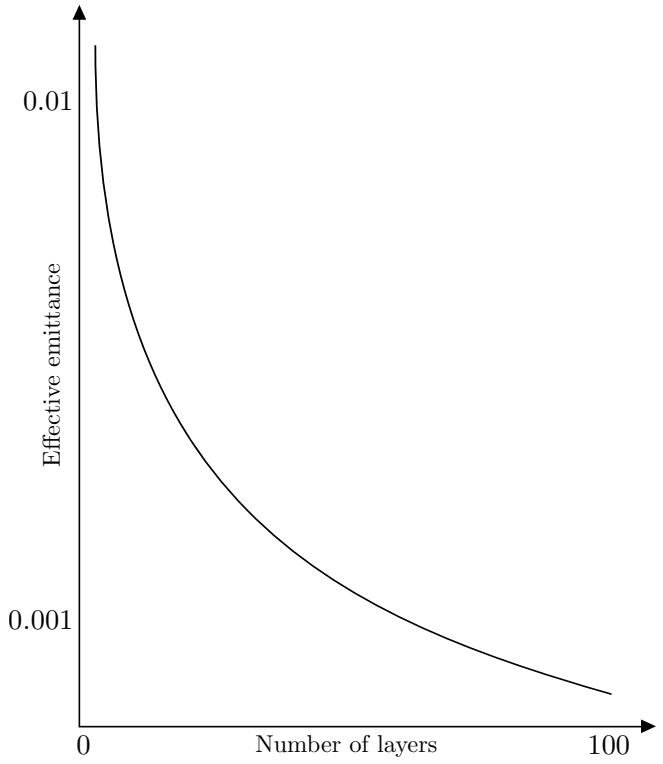

Figure 1.4: Theoretical effective emittance versus number of layers

This consist typically of several layers of aluminized plastic film, such as Mylar or Kapton, acting as radiative shields, each separated by a low conductance spacer (e.g. silk, Nylon or a glass fiber net). Such a blanket might consist of 40 or more layers, each about 10 μm thick and aluminized

on both sides. The theoretical values of effective emittance as a function of number of layers, neglecting the effect of conduction between layers or through joints, or edge effects, are shown in figure 1.4.

Anyhow, due to the difficult standardization of space missions, it is impossible to determinate the best way to control radiators efficiency: any of the presented devices have advantages and inherent issues that, depending on the type, could affect all the satellite subsystems. Therefore, the choice between these devices is done to obtain a highly optimized solution, which represent the best trade-off between power consumption, mass and development complexity, considering the mission requirements and its thermal environment.

1.4 State of the art

The heat amount exchanged by a radiator strongly depends both on the internal heat fluxes and on the thermal environment that the satellite faces, and its sizing must be carefully calculated in order to ensure the right dissipation in the worst hot case, namely the one with maximum internal and external heat fluxes. Anyhow, given that these two fluxes may vary quite a lot during the mission lifetime (i.e. during electronics switching off, eclipses, attitude variation, surfaces degradation) an accurate design has to be chosen in order to obtain an opportune flexibility on the radiator performances, so that it would not exchange too much heat and over-cool the electronics.

A great example of a modern radiator is the one built for Rosetta: this probe is orbiting its target Comet 67P/Churyumov-Gerasimenko, whose orbit reached its closest point to the Sun on 13 August 2015. But to make that rendezvous involved a decade-long odyssey of planetary flybys and wide temperature fluctuations. At times Rosetta urgently needed to dump waste heat, while at other points heat became a precious resource, essential to keep the mission from freezing during its 31-month hibernation phase. The solu-

tion was a particular louver radiator (visible in figure 1.5), with many thin reflective metal blades. In high temperature conditions they remain open to let heat radiate away, but in the cold they automatically close up instead. Some 14 of these louver panels cover 2.25 m^2 of Rosetta, placed over its radiators across the side and back of the spacecraft. The louvers open and close on a fully passive basis, requiring no power to operate. Instead they work on a bimetallic thermostat principle. The blades are moved by coiled springs made up in this case of a trio of different metals that expand and contract at differing rates, precisely tailored to rotate as required.

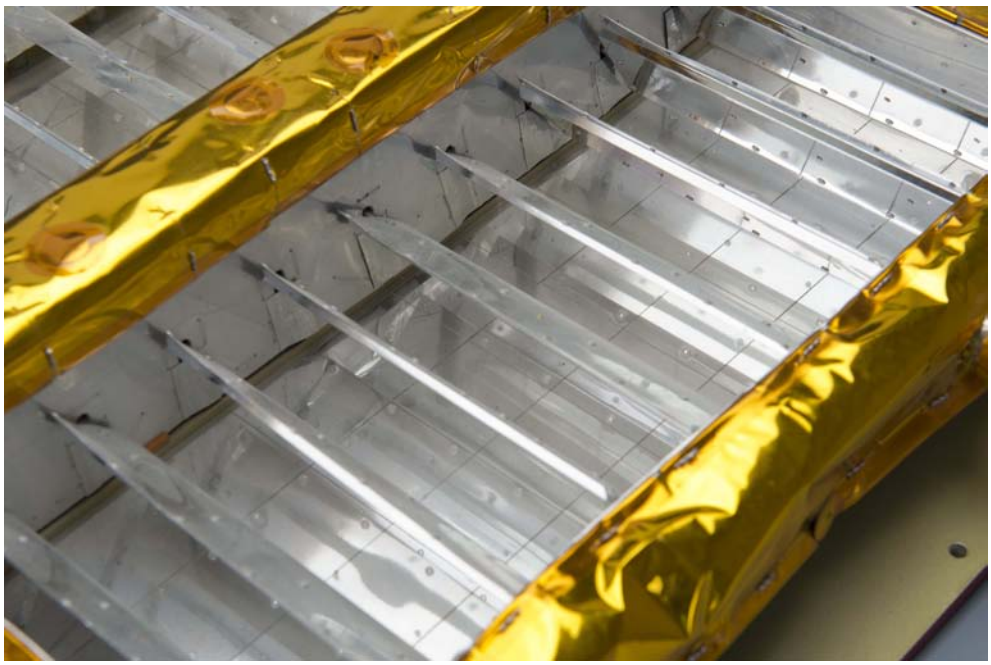

Figure 1.5: Picture of the Rosetta thermal louvers. Copyright ESA-A. Le Floc'h

Another great example of smart engineering solutions is the BepiColombo Mercury Planetary Orbiter (MPO) TCS. In fact it will challenging harsh thermal environment while in orbit around Mercury. Not only will it be strongly illuminated by the Sun, it will also orbit closer to its host planet than previous spacecraft and will therefore experience much higher levels of

infrared radiation on its nadir-pointing panel. To cope with these demands, the MPO is fitted with two sets of multi-layer thermal insulation blankets, while it is equipped with a very large radiator to transfer the heat generated by its internal systems to deep space. Heat from the electronics units inside the spacecraft is carried to the radiator by 93 heat pipes, the majority of which are embedded in the internal structural panels. The radiator takes up one entire panel of the spacecraft. It is protected from infrared radiation coming from Mercury by polished titanium louvers that reflect the incident radiation into space. The louvers will reach a temperature of around 680 K, while the radiator will operate at 330 K.

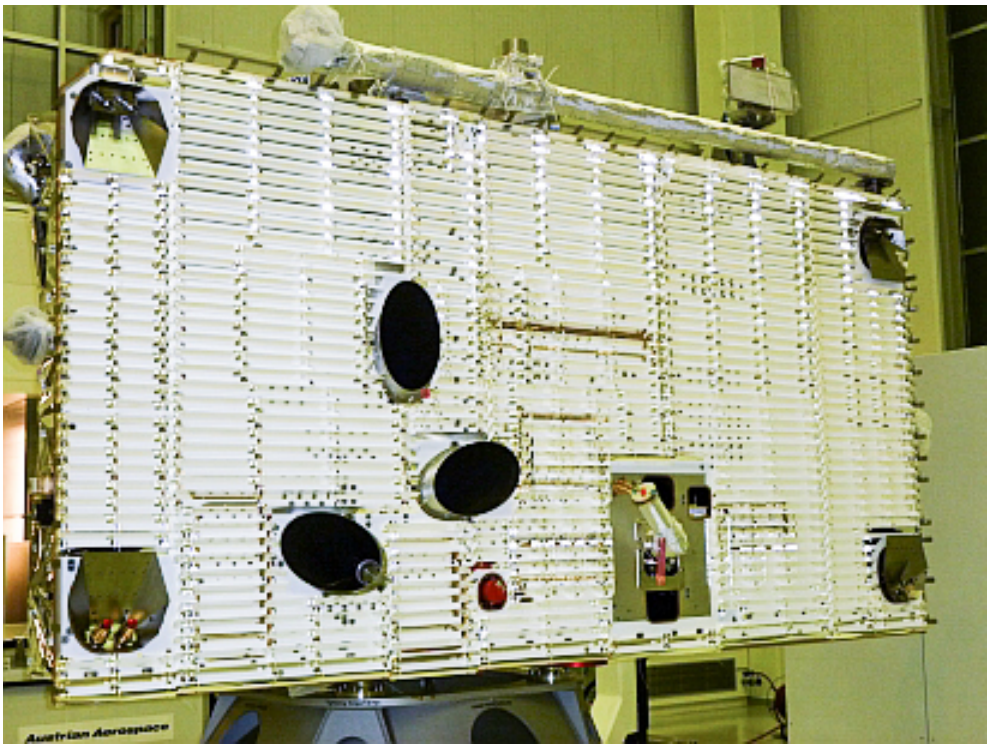

Figure 1.6: Picture of the MPO radiator. Credit: ESA

A different solution has been approached the NASA MESSENGER mission, a probe that orbited the planet Mercury between 2011 and 2015. While orbiting Mercury, MESSENGER will feel significantly hotter than spacecraft

that orbit Earth, because the Sun shines up to 11 times brighter at Mercury than we see from our own planet. MESSENGER first line of thermal defense is a heat-resistant and highly reflective sunshade[8], fixed on a titanium frame to the front of the spacecraft, as it is possible to see in figure 1.7. Measuring about 2.5 meters tall and 2 meters across, the thin shade has front and back layers of Nextel ceramic cloth surrounding several inner layers of Kapton plastic insulation. While temperatures on the front of the shade could reach 640 K when Mercury is closest to the Sun, behind it the spacecraft will operate at room temperature, around 290 K. Multilayered insulation covers most of the spacecraft. Radiators and one-way heat pipes are installed to carry heat away from the spacecraft body, and the orbit is designed to limit the spacecraft exposure to heat re-radiating from the surface of Mercury. The combination of the sunshade, thermal blanketing and heat-radiation system allows the spacecraft to operate without special high-temperature electronics.

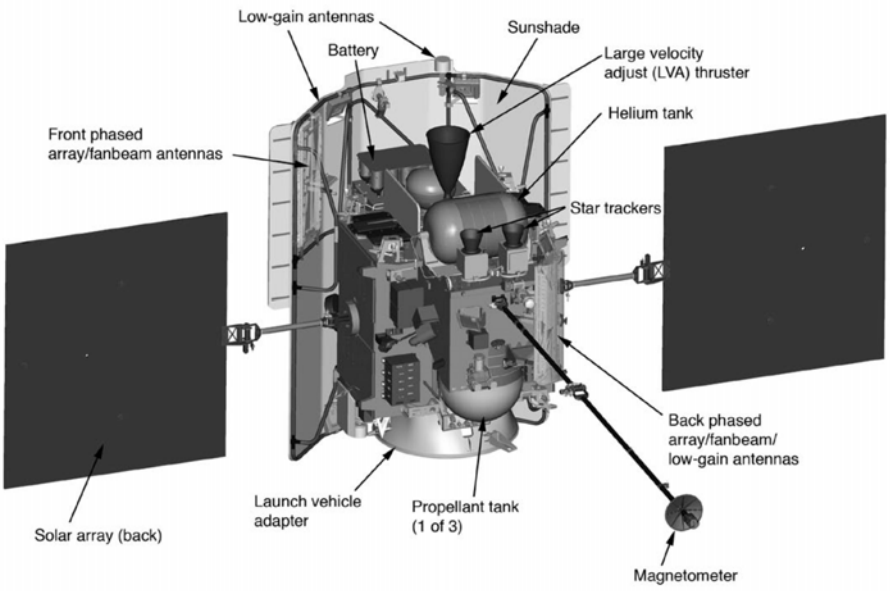

Figure 1.7: Drawing of the MESSENGER probe. Credit: NASA

Nevertheless, even in the space qualified state-of-art strategies, it is pos-

sible to identify a lack in the radiators methods of control: in fact does not exist a device which permits a simple, low-power control that is also strongly-manageable by the designer, preferably through a command. In this framework, the next chapters will present a new concept of heat radiator, which is named *multi-plate* and has been designed in order to fill that gap.

Chapter 2

Multi plate radiator

2.1 POLARIS Experiment

The mission of POLARIS[13] experiment was to demonstrate the feasibility of a new concept of heat radiator, which allows active thermal control through an innovative working principle based on a geometry change. Moreover, even if this radiator concept could work with any kind of linear actuation, it has been decided to use dielectric elastomers actuators, due to their advantages in a space environment (such as a very low power consumption and a great reliability) and in order to make the experiment more interesting and challenging; however this detail of the experiment will be overlooked in this essay in order to better analyze the radiator itself.

The three plates that compose this radiator are the most important part of the experiment. They provide an innovative way to exchange heat from the inner box to the external environment; they are squared, metallic and, in order to achieve the best thermal conductivity, with a surface as flat as possible. Moreover, due to inevitable surfaces imperfections, thin thermal conductive pads are interposed between the plates. The three plates are independent each other, and in order to allow a correct functioning of the radiator they have one controlled degree of freedom: the second and the third

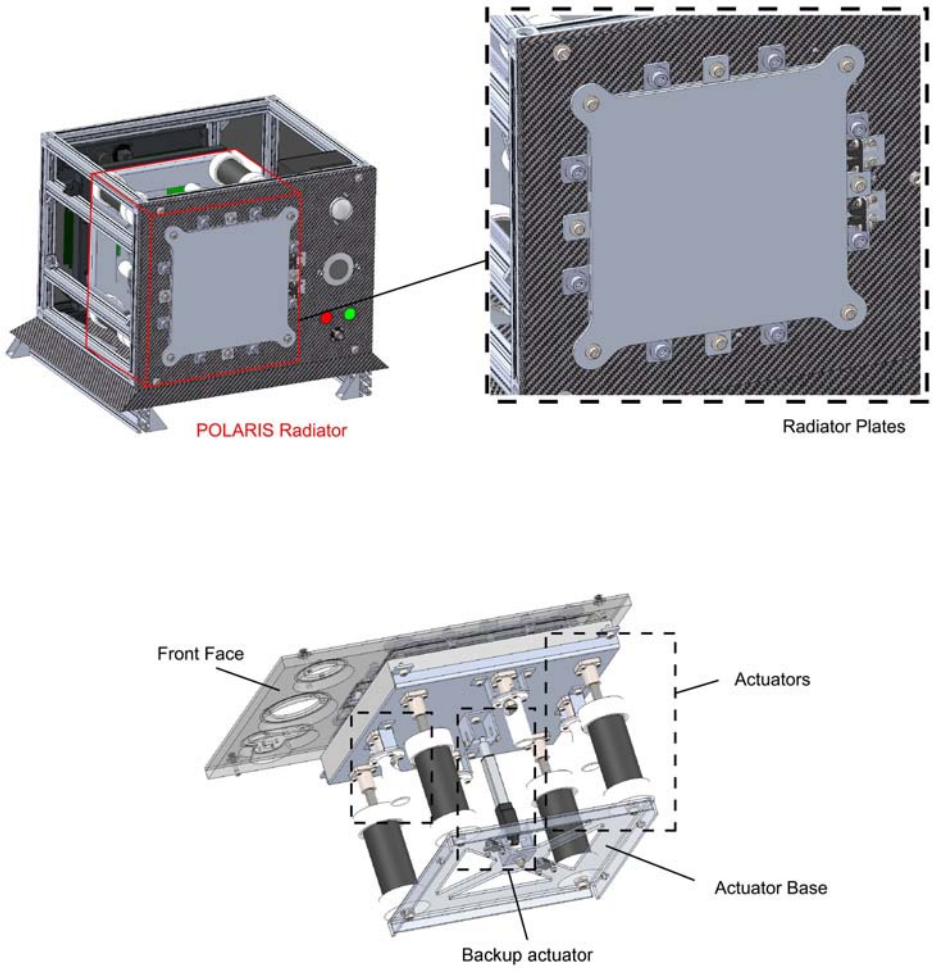

Figure 2.1: Drawing of the experiment setup

plate are constrained to a system of non-conductive rods and, through the pushing of these rods, plates can be moved (only the first plate is fixed to the structure).

Basically, the three parallel metallic plates are linked together and constrained so that an actuation system (composed by DE actuators, pre-compressed springs and a linear actuator) can separate them or put them in good thermal contact. In order to simulate the heat generation of a real payload, multiple power resistors are connected behind the first plate of the radiator to act as a Dummy Payload (DP).

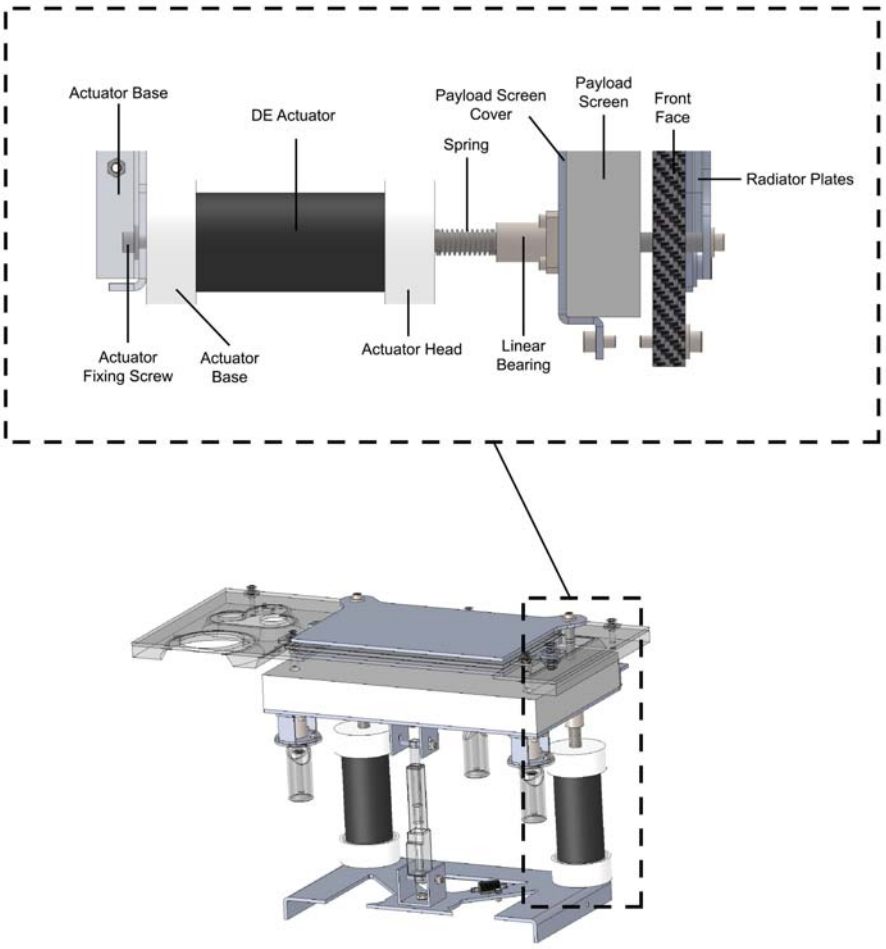

Figure 2.2: Detail of the actuation mechanism

It is possible to identify three different configurations (called hereafter *states*) with this particular setup:

- **State 1** The three plates are in contact. When the DE actuators are used, the springs interposed between the actuators heads and the linear bearings ensure the adequate pressure between the plates and this can

ensure a good conductive path in order to make them work almost as a single plate. However, when the electric linear actuator is used, it is responsible of the pressure applied to the plates since it moves the baseplate where the DE actuators are mounted on. In this state, the internally generated heat is transferred through the plates mainly by conduction and then radiated to the environment by the external plate. This condition is favorable to the heat exchange.

- **State 2** The first and the mid plate are no longer in contact. In this configuration only the mid and the external plate are in contact. Therefore, between the first and mid plate there is a radiative link (the thermal resistance increases), while between the mid and the external plate remains the conductive link. The heat exchange is lowered compared with the previous configuration. This state has not been tested extensively as the other two, since the pressure between the external and the median plate is much lower than in state one and is less controllable.

- **State 3** In this configuration the external plate is separated from the mid plate. Between the two gaps obtained through the three plates separation there is a radiative link and the heat exchange reaches its minimum value. To achieve this state the DE actuators have to extend or the linear actuator have to shorten; the mechanism is showed in figures 2.1 and 2.2.

The actuations are controlled by the on-board Single Board Computer (SBC) that, thanks to the copious number of sensors that constantly monitor POLARIS, is able to automatically alternate between states. The switch between these three conditions allows to vary the system equivalent thermal resistance; therefore it is possible to control the heat dissipated toward the environment. Moreover, since it is very difficult to measure the exact amount of heat dissipated by the whole electronics system, the radiator will exchange

only the heat generated by a power resistor, which act as a DP as described before.

In such a context, the experiment setup consists in a box divided (conceptually and physically) in two different parts:

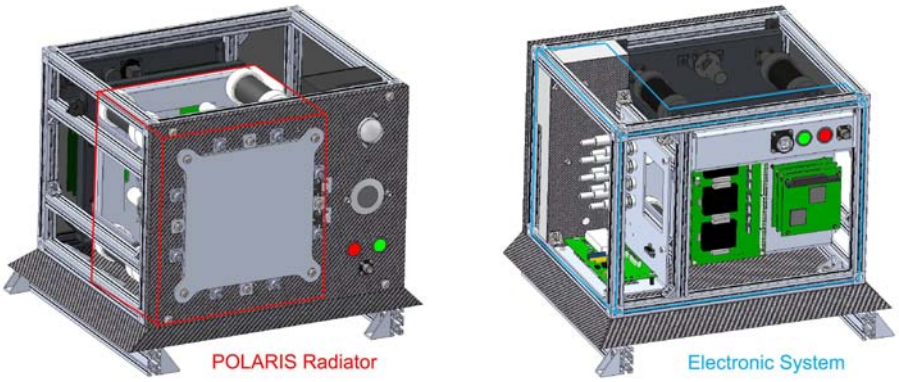

Figure 2.3: Focus on the experiment parts

1. **POLARIS Radiator** It contains most of the sensors, the DP and the three radiator plates (whose last is exposed to the environment); the plates and the DP are thermally insulated from the rest of the experiment. Also, it contains both the polymeric actuation system and the backup one (a Firgelli® L12 electrical linear actuator).

2. **Electronic System** It contains the SBC, the data acquisition devices, the Printed Circuit Boards (PCBs) and the power supply system. Its main goal is to monitor the temperature sensors that are placed on the whole experiment (especially in the POLARIS radiator) and are extremely important in order to characterize the radiator performances. These sensors are also needed in order to estimate the dummy payload temperature during the various phases predicted during the stratospheric flight. Temperature sensors are also mounted on many other components in order to verify that each one operates in its temperature range. With these data the SBC determines if it is necessary to power

on the experiment internal heaters. Temperature and pressure sensors also characterize the outer environment during all the flight phases. Optical interrupters are placed on the experiment front face in order to check the effective plates separation and two radiometers (pyranometer and pirgeometer) collect data about the IR-Visible incoming radiation (and the resulting thermal loads) during the whole flight. The data sampling, the data storage and the transmission to the ground station is managed by the on board SBC.

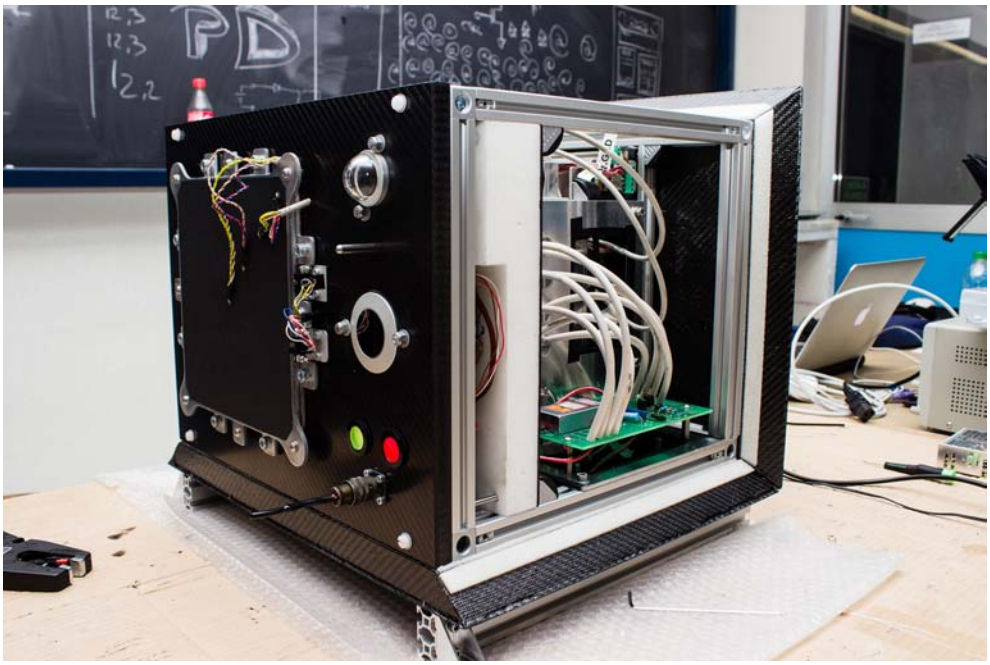

Figure 2.4: Picture of the experiment setup

For a more accurate description of the POLARIS experiment please refer to the Student Experiment Documentation (SED [13]) drafted during the BEXUS programme.

2.2 Theoretical background

A theoretical background is depicted here[1]; in fact many equations are needed to explain the behavior of a multi-plate radiator, as schematized in figure 2.5. The heat exchange from the external plate to the environment can be assimilated to the radiative heat exchange; thus it will be considered:

- G = Irradiation: the total radiative specific flux reaching the surface
- B = Radiance: the total radiative specific flux (inclusive of the flux emitted and the reflected fraction of the incoming one)
- E = The global black-body emission value at a given temperature

According to these definitions and considering A the interested area, it is possible to write equations 2.1 and 2.2.

$$B = \varepsilon\, E + (1 - \varepsilon)\, G \tag{2.1}$$

$$q = A \cdot (G - B) \tag{2.2}$$

Considering two plane parallel plates exchanging flux one to each other, the total radiative power is 2.3. Moreover, in radiative heat transfer, we consider the configuration factor $CF_{A\to B}$ as the proportion of radiation which leaves surface A and reaches surface B .

$$q_{1-2} = B_1 \cdot A_1 \cdot CF_{1-2} - B_2 \cdot A_2 \cdot CF_{2-1} \tag{2.3}$$

Assuming that $A_1 \cdot CF_{1-2} = A_2 \cdot CF_{2-1}$, the equation 2.2 can be re written as follows:

$$q_{1-2} = \frac{B_1 - B_2}{1/_{A_1 \cdot CF_{1-2}}} = \frac{B_1 - B_2}{1/_{A_2 \cdot CF_{2-1}}} \tag{2.4}$$

Then, considering the equations 2.1 to 2.4, it is possible to write the 2.5.

$$q_{1-2} = \frac{E_1 - E_2}{{}^{1-\varepsilon_1}/_{\varepsilon_1 A_1} - {}^{1}/_{A_1 CF_{1-2}} + {}^{1-\varepsilon_2}/_{\varepsilon_2 A_2}} \tag{2.5}$$

Now, assuming $CF_{1-2} = CF_{2-1} = 1$ and $A_1 = A_2 = A$ it is possible to obtain the equation describing the flux between one plate to another:

$$q = \frac{A \cdot \sigma \cdot (T_1^4 - T_2^4)}{{}^{1}/_{\varepsilon_1} + {}^{1}/_{\varepsilon_2} - 1} \tag{2.6}$$

Where ε is the plate emissivity and σ is the Stefan-Boltzmann constant. The value of the $CF_{int \to ext}$ between the two directly opposed plates is set with good approximation to 1[6]. If an opaque screen s is interposed in between the two plates, at the equilibrium, it will reach the temperature T_s needed to match the fluxes in equation 2.7 and 2.8. This is the concept behind the multi plate radiator, and will be fundamental to understand how POLARIS works[1].

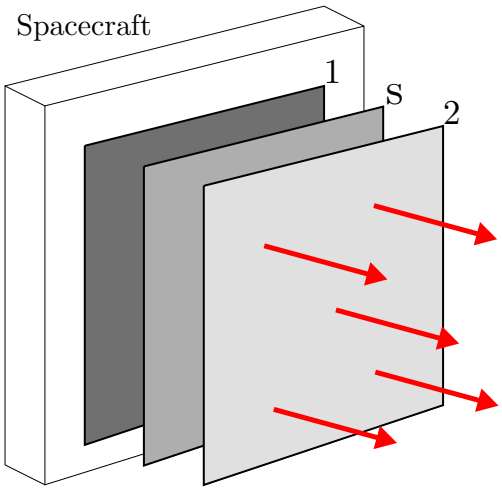

Figure 2.5: Schematic of the multi plate configuration

$$q_{1-s} = \frac{A \cdot \sigma \cdot (T_1^4 - T_s^4)}{{}^{1}/_{\varepsilon_1} + {}^{1}/_{\varepsilon_s} - 1} \tag{2.7}$$

[1]What is POLARIS and how it works is explained in section 2.1

$$q_{2-s} = \frac{A \cdot \sigma \cdot (T_s^4 - T_2^4)}{{}^1\!/_{\varepsilon_s} + {}^1\!/_{\varepsilon_2} - 1} \tag{2.8}$$

Assuming $\varepsilon_1 = \varepsilon_2 = \varepsilon$ it is possible to obtain the equations:

$$T_s^4 = \frac{1}{2}(T_1^4 + T_2^4) \tag{2.9}$$

$$q = \frac{1}{2}\frac{A \cdot \sigma \cdot (T_1^4 - T_2^4)}{{}^2\!/_{\varepsilon} - 1} \tag{2.10}$$

Comparing the latter with the same equation obtained without the screen it is possible to see that the flux is halved. Moreover, it is possible to extend the equation for different number m of screens:

$$\left(\frac{q}{A}\right)_{\substack{with \\ screens}} = \frac{1}{m+1}\left(\frac{q}{A}\right)_{\substack{without \\ screens}} \tag{2.11}$$

From this equation is possible to understand the working principle behind the POLARIS radiator concept: the tightened plates configuration could be assumed as a single plate emission, instead the separated plates configuration could be assumed as a single plate emission with m screens. More in detail, in the tightened plates configuration the plates are in contact and there is a conductive link between them; this drives to a lower equivalent thermal resistance that maximize the heat exchange. In the open configuration plates are no more in contact and there is a radiative link between them; this leads to a higher equivalent thermal resistance that minimize the heat exchange. Thus, switching between these two configurations is possible to modulate the heat exchange.

In the simulations described in section 2.3, it is possible to calculate the radiator resistance in state 1 as the sum of the plate resistance R_{plate} and the gap filler resistance R_{pad}:

$$R_{close} = n \cdot R_{plate} + (n-1) \cdot R_{pad} \tag{2.12}$$

Where n is the variable number of plates. Therefore, with T_{int} the temperature on the internal face of the first plate and T_{ext} the temperature on the external face of the last plate, the flux is:

$$q_{close} = \frac{A_{plate} \cdot (T_{int} - T_{ext})}{R_{close}} \tag{2.13}$$

To better understand the radiators performances in state 3, it is possible to calculate an average equivalent thermal resistance. This one varies depending on the two radiating plates' absolute temperatures and involves an approximation related to the ΔT between the plates themselves. As explained before, the heat exchange between one plate to another in open condition can be assumed as:

$$q_{open} = \frac{4 \cdot A_{plate} \cdot \sigma \cdot (T_1^4 - T_2^4)}{{}^1\!/_{\varepsilon_1} + {}^1\!/_{\varepsilon_2} - 1} \tag{2.14}$$

This equation can be linearised if the temperature T_1 and T_2 are similar. In fact, with a few algebraic, it is possible to assume T_m as the arithmetic mean of T_1 and T_2 and the formula becomes:

$$q_{open} = \frac{4 \cdot A_{plate} \cdot \sigma \cdot T_m^3 \cdot (T_1 - T_2)}{{}^1\!/_{\varepsilon_1} + {}^1\!/_{\varepsilon_2} - 1} \tag{2.15}$$

So the equivalent thermal resistance can be assumed as:

$$R_{open} = \frac{{}^1\!/_{\varepsilon_1} + {}^1\!/_{\varepsilon_2} - 1}{4 \cdot \sigma \cdot T_m^3} \tag{2.16}$$

As it is possible to see, the equivalent thermal resistance is not a given value, but changes depending on the two radiating plates' absolute temperatures. However, in every useful temperature scenario, it is correct to assume:

$$R_{open} \ll R_{close} \tag{2.17}$$

In this way, the global flux that passes through the radiator is much lower than the one in the closed configuration, isolating the payload from the external environment. Furthermore, the conductive link towards the

air that lies between the plates has been added in order to find the most efficient plates distance. In fact the optimal plates' open configuration is a trade off because increasing the plates' distance will decrease the conductive flux towards the air, but boosts the radiative one by means of CF change.

On first approximation, only the external face of the last plate is thermally connected with the environment and is able to exchange radiative and convective heat fluxes. It is here neglected any other thermal path toward the external environment. In order to evaluate environment average conditions, was initially used the International Standard Atmosphere (ISA)[3] model, which includes pressure, temperature, density and viscosity at different altitudes. However, this model shows many issues when used to extrapolate data over 20 km (this issue will be clarified later). For this reason, atmospheric data have been obtained from the previous BEXUS flights, in particular the BEXUS 9, 10, 11, 16 and 17. The convection heat transfer coefficient α has been computed through the average Nusselt number Nu_L supposing a laminar flow over a flat plate. Thus, convective heat flux toward the plate can be computed as:

$$q = \alpha \, A_{plate} \, (T_{amb} - T_{plate}) \tag{2.18}$$

Net radiative heat flux has been computed as the difference between the incoming and the outgoing radiation. Outgoing radiation could be directly computed with the surface temperature:

$$q = \sigma \, \varepsilon \, A \, T_{plate}^4 \tag{2.19}$$

On the other side, incoming radiation had to be calculated as the sum of fluxes coming from Sun, Earth and the sky. A random BEXUS gondola movement, approximated as a periodic rotation around its vertical axis, has been implemented in order to simulate an intermittent exposure of the external surface to sunlight.

2.3 Thermal simulation

An accurate thermal numerical simulation has been developed in Matlab® environment and is based on the divided differences method. It is able to calculate the temperature of the radiator plates and the DP depending on the internal power load and the external fluxes. Moreover, the simulation computes both the CF with sky and Earth surface during a simulated BEXUS flight. The simulation was fundamental to fix the design drivers (plates dimension and number, DP power consumption, sensors needed, etc.) in order to build the best possible experiment setup. Some outputs are visible in the following images, but only few words will be spent, in order to move up to the experiment real behavior.

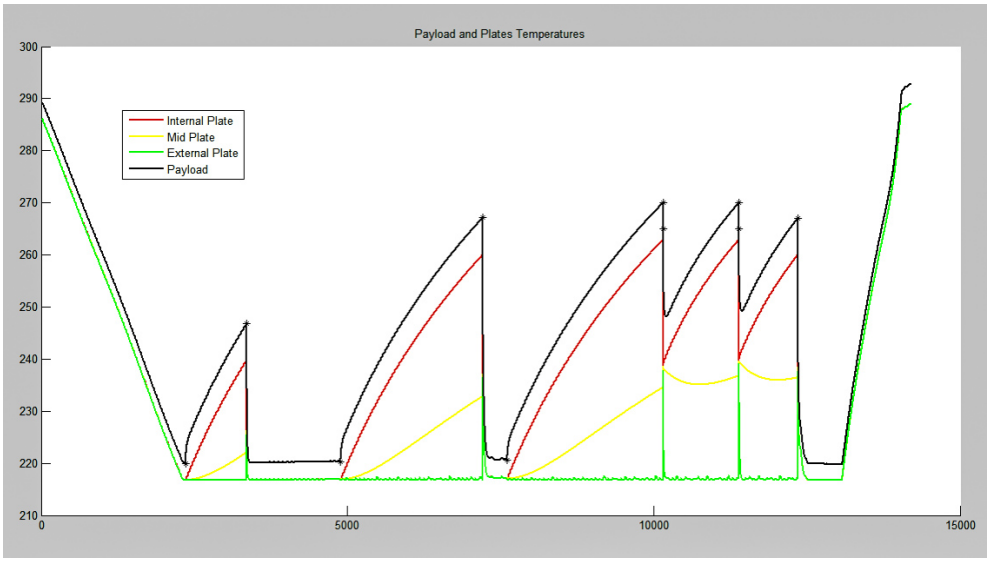

Figure 2.6: Example of thermal simulation

In the figure 2.6 it is possible to see the radiator temperature during the flight; in fact it is plotted the temperature in K vs the time in s. In this simulated flight the radiator performed only five switches between state 1 and state 3. Instead, in figure 2.7, a more complex flight simulation has been carried. The latter is more similar to the real flight test, where many different

phases were identified and different tests has been done. In both pictures on the left side of the diagram it is possible to notice a constant temperature decreasing: this is the *ascending phase*, where the experiment take off from ground and reaches the operative altitude at 30 km. On the other hand on the right side there is an equivalent *descending phase*. The black line represents the DP temperature, while the green, red and yellow lines are the average temperatures of the radiator plates, as described in legend.

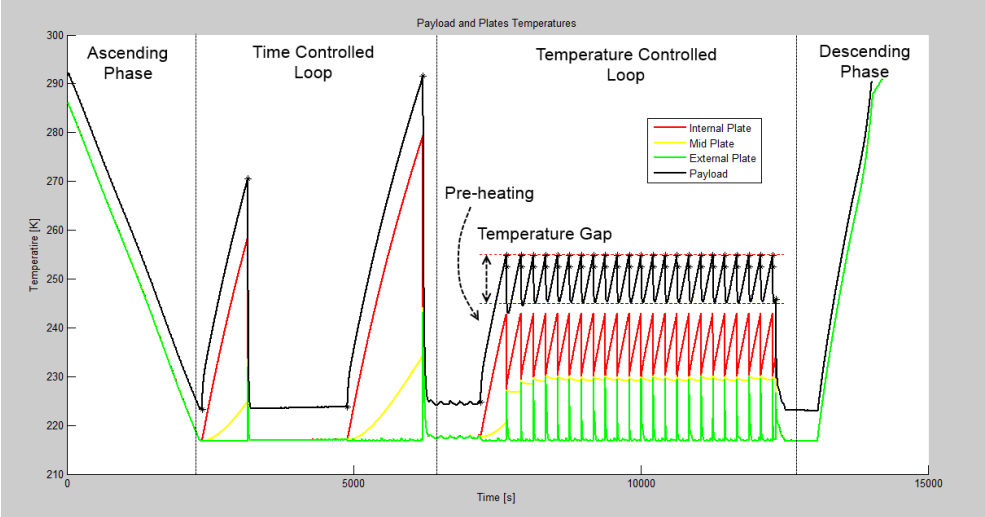

Figure 2.7: Example of thermal simulation (whole BEXUS flight)

Furthermore, also the temperature distribution over the three plates was simulated. This has been done in order to justify the number and the position of temperature sensors on the radiator plates. This made possible a better evaluation of the experiment performance.

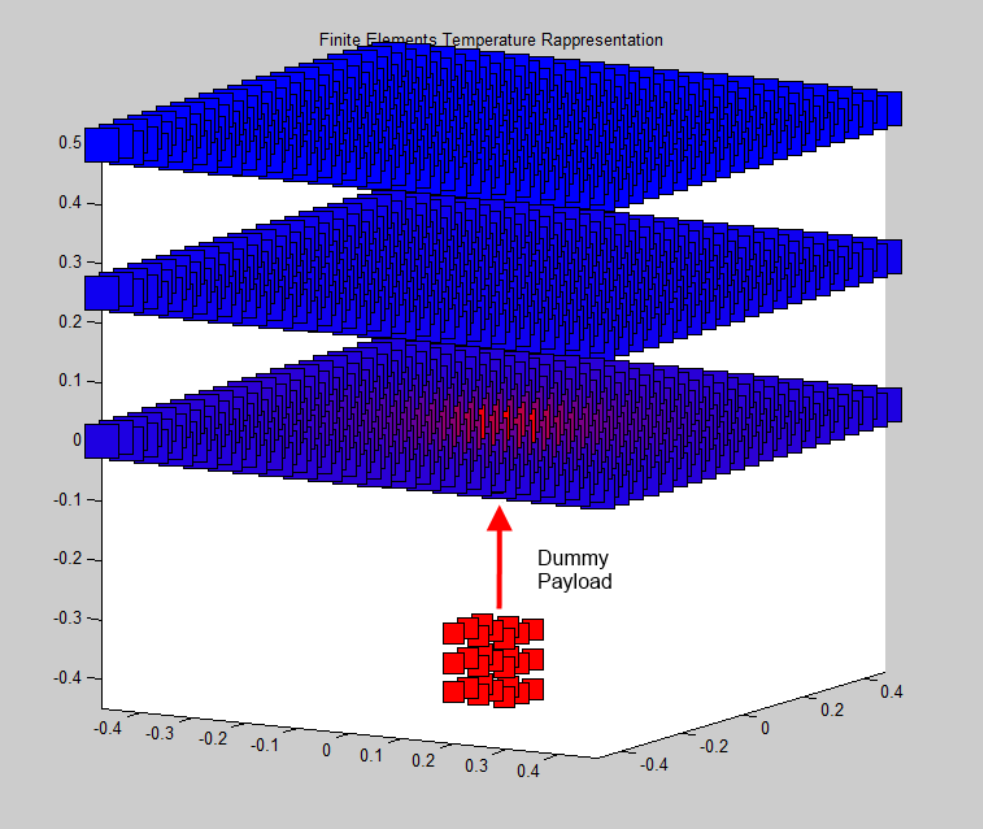

Figure 2.8: Temperature distribution over radiator plates, simulated

Chapter 3

Laboratory test

3.1 Testing setup

All the tests described in this chapter have been carried out in the CISAS facilities in Padova. In particular, the vacuum chamber used to simulate the pressure faced by POLARIS in stratosphere is part of the two-stage light-gas gun designed for hypervelocity impact experiments. The downside of this facility is the impossibility to simulate the thermal condition present in stratosphere; by the way the temperature in the laboratory was controlled and fixed to approximately $26° \ C$ $(299 \ K)$, but more details will be given with each test result.

The sensors used to monitor the pressure inside the chamber were the ones assembled in POLARIS. Those are two identical Honeywell "TruStability®" ($HSCDANN1.6BAAA5$) piezoresistive silicon absolute sensors capable to read between 0 to 1.6 *bar*. Those were previously calibrated with another, way more precise, pressure transducer and have a maximum rated total error of $\pm 1\%$. In order to calibrate those pressure sensors it was assumed that the behavior of the sensing unit was linear, as described by the producer. Then, input and output points were taken with the calibrated and the non calibrated units in order to find the calibration coefficients m and c to include

Figure 3.1: The experiment power supply and the notebook running the ground-segment software during the test campaign in the CISAS vacuum chamber

in equation 3.1.

$$y = m \cdot x + c \tag{3.1}$$

Those correlations were implemented in the on-board computer so that the experiment was able to display and store the right output y as a function of x during the measurement process; this has been extended to any stimulus in the desirable range, not only at the points used during the calibration but anywhere in-between: very rarely sensors contain singularities.

To sense temperatures the choice relapsed on Resistance Temperature Detectors (RTD). This term is usually pertinent to metal sensors fabricated in the form of either a wire or a thin film. Temperature dependence of resistivity of all metals and most alloys gives an opportunity to use them for temperature sensing[4]. While virtually all metals can be employed for sensing, platinum is used almost exclusively because of its predictable response, long-term stability, and durability. The temperature inside and outside the

experiment is then detected by a couple of class B[1] LabFacility Pt100 probes, capable to measure in the temperature range bwtween $-200°C$ to $+650°C$. These sensors have the platinum coil inside an alumina ceramic body, making them sturdier than the Pt100 used on the plates. In fact those are tiny class A IST "MiniSens" Pt100 ($P0K1.161.6W.Y.010$) chosen to precisely measure the temperature over different spots of the radiator plates. Moreover, thank to their size, they condition at the least the radiator performance. Even if their operative temperature range is reduced between $-90°C$ to $+300°C$ they have a longer term stability and a much lower response time. All the sensors outputs are computed in the experiment in order to to take into account the single sensors properties. The formula 3.2 has been used when sensing temperatures lower than $0\,°C$, while the 3.3 for the positive temperatures. The constants A, B, and C are determined by the properties of platinum used in the construction of the sensor and are given by the manufacturer.

$$R_t = R_0 \left[1 + At + Bt^2 + Ct^3(t - 100)\right] \tag{3.2}$$

$$R_t = R_0 \left[1 + At + Bt^2\right] \tag{3.3}$$

The temperature is then converted in K in the SBC before any further calculation. Another approximation has been tried out: the Callendar-van Dusen (described in equation 3.4).

$$R_t = R_0 \left\{1 + \alpha \left[1 - \delta(\frac{t}{100})(\frac{t}{100} - 1) - \beta(\frac{t}{100})^3(\frac{t}{100} - 1)\right]\right\} \tag{3.4}$$

The value of δ is obtained by calibration at a high temperature and β is obtained at the calibration at a negative temperature. However, the com-

[1]The European standard, also known as the DIN or IEC standard, is considered the world-wide standard for Pt100. This standard requires the RTD to have an electrical resistance of 100.00 Ω at $0°C$ and a temperature coefficient of resistance (α) of 0.00385 $\Omega/\Omega/°C$ between 0 and $100°C$. Class A sensors have a tolerance of $\pm\,(0.10 + 0.0017 \cdot t)^\circ\,C$, while class B sensors have a tolerance of $\pm\,(0.30 + 0.0050 \cdot t)^\circ\,C$.

puted temperature was the same, so the two separate approximations 3.3 and 3.2 were maintained.

In order to better understand the real behavior of the radiator, two other sensors have been recognized essential. In fact it is very difficult to evaluate precisely the amount of thermal loads coming from the environment and so two radiometers were placed on the front face of the experiment, just beside the radiator plates. Those two sensors were built and calibrated in the Delta OHM laboratories in Padova. This is an accredited calibration laboratory [2] which provided the POLARIS experiment with an LP Pyra03 piranometer and a LP Pirg01 pyrgeometer, capable of measure respectively the amount of incoming visible and IR radiation.

Figure 3.2: The experiment in the vacuum chamber

These use a thermopile as sensitive unit, so they belong to a class of PIR detectors. Their operating principle is the same as that of a thermocouple.

[2]Delta OHM develops and manufactures instruments for measuring temperature, humidity, pressure, air speed, light, acoustic and vibration, air quality, multifunction instruments, data loggers, environmental and water analysis. The calibration Accredia Lat $N°$.124 laboratory of Delta OHM is accredited in metrology for many physical quantities

A single thermocouple is a low-sensitivity device responding with tens of microvolts per $1K$ change. In a thermal-radiation sensor, temperature change of the sensing element when exposed to the object is very small; thus, a stronger sensor response is required. This is achieved by increasing a number of thermocouples that makes a thermopile (piling up). The frame is thermally coupled with a reference temperature sensor. This is needed in particular for the piranometer, in order to compute the net irradiation, as described in equation 3.5. Here E is the radiation stated in W/m^2, C is a calibration factor and U_{out} is the output signal of the sensor in μV.

$$E = \frac{U_{out}}{C} + \sigma \cdot \ T_{sensor}^4 \tag{3.5}$$

All the sensors are connected to two Sensoray model 518, capable to read various analog and digital signals. One of the two Sensoray boards is dedicated to the radiator temperature measurements, employing 8 class A Pt100 RTD, connected in 4-wire configuration. Class A RTDs provide $0.33°C$ accuracy at $-90°C$ while the Sensoray 518 provides $0.2°C$ accuracy. Thus, the worst case overall accuracy is about $0.5°C$.

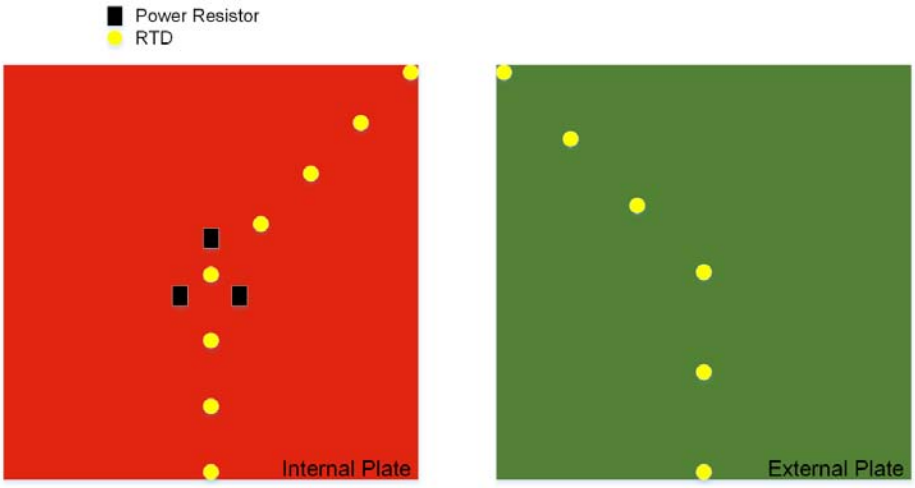

Figure 3.3: Drawing of the RTDs and the DP disposition over the radiator plates

In figure 3.3 it is shown the RTD disposition over the radiator plates; this disposition, accordingly to the simulations results (section 2.3), is the most efficient to observe the temperature gradient of the plates[3].

The power consumption of the DP is precisely monitored by a watt-meter, so it is possible to directly compute the heat load towards the radiator. The three power resistors that act as DP are plate-mounted $100 \pm 0.1\%\ \Omega$ thick film resistors and during most of the test their dissipated power was $\sim 9\ W$, but the precise values will be given with every individual test.

Figure 3.4: Example of the software GUI of the experiment

All the sensors data, once acquired and elaborated by the two Sensorays, are both stored inside the experiment and sent to an external computer by the SBC. Through the custom software GUI it is possible not only to monitor and record all the data coming from the experiment, but also to switch between the different states (as described in section 2.1) and manually

[3]Due to some issues with the multiplexing board, the number of RTDs utilized to monitor the temperature gradient over the plates has been decreased to 8 (4 for each plate). Further information is reported in the SED

override other automated actions if something goes wrong. In figure 3.4 it is shown an example of the software GUI programmed specifically for the POLARIS experiment.

3.2 Test results

> Hofstadter's Law: It always takes longer than you expect, even when you take into account Hofstadter's Law.
>
> Douglas Hofstadter

A single run of the experiment consist in roughly two and a half hours of data acquisition, where a single heater (the one acting as DP) was turned on and the plates were fixed in a determined state. In order to exclude as many variables as possible, only the equilibrium state was the objective of those tests. In fact, during the switching operations, a great role is played by the thermal capacity of the aluminum plates. However, since in future developments the thickness of the plates will be reduced as much as possible, this element have been excluded by the calculations.

This leaded to acquire the so-called *steady-state* condition for each state. The power dissipated by the DP was constantly monitored and was always oscillating between 8.96 to 8.98W. An example of the DP temperature profile can be found in figure 3.5, please note that the time is shown ten time bigger due to the 10 Hz data acquisition frequency. Since physically there is not a real payload, the DP temperature is the temperature sensed by the Pt100 which is nearest to the power resistor that is turned on. Other analysis, such as the temperature difference between the internal and the external radiator plate, will be better examined in section 5.

This measurement does not consider the environment temperature. In fact, even if the AC unit in the laboratory was always turned on, a small

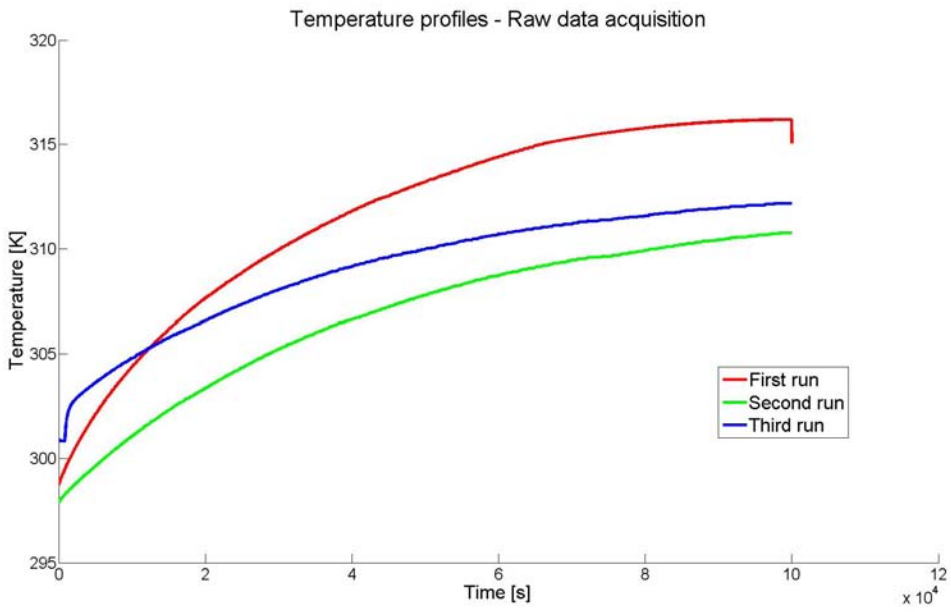

Figure 3.5: Example of raw temperature data from three different tests

change in room temperature was inevitable. It is, however, possible to normalize the radiator temperature with the ambient one, constantly monitored by the experiment inside the vacuum chamber. As it is shown in figure 3.6, the gaps are much tighter. This passage consist in a simple difference between the two temperatures and is a licit transition since we decided to compute the thermal fluxes only as a function of ΔT, as described in equation 2.15. In order to compute the equivalent thermal resistance in state 3, the proper T_m will be considered, so the error will be negligible (as little as 0.1%). Moreover, in figure 3.6 is more emphasized the difference between the *first run* and the *third run*; in fact during the first run the radiator was in state 3, while in the second and the third it was in state 1.

In figure 3.7 data of multiple measurements are computed and only an average value is showed (normalized as described before). This is the most explanatory result, in fact it is possible to appreciate the difference between the radiator in state 1 (which behavior is drawn in green) and in state 3 (in

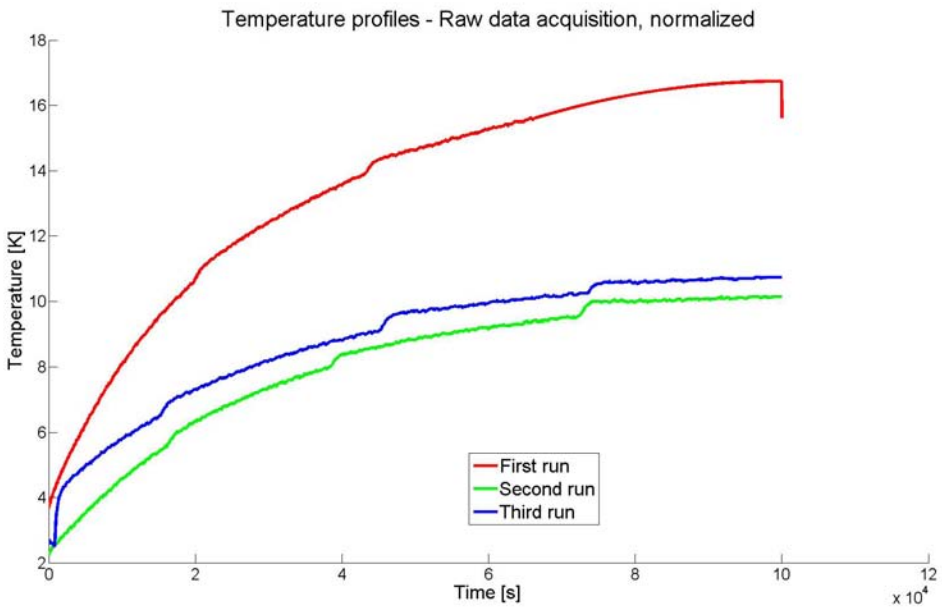

Figure 3.6: Normalized temperature data from three different tests

red). At first glance it is noticeable that in the closed plates configuration the DP temperature is 10.89 K higher than the ambient one, while during the open plates test it is 16.65 K higher; further considerations on this will be made in section 5. The disturbances on the plot are due to the little change in temperature caused by the decompression of the vacuum chamber. In fact the chamber is not perfectly airtight and the user have to manually turn on the pump to decrease the pressure when it is too high. While the pump is pulling out air the remaining gas in the chamber withstand an adiabatic expansion, thus lowering the gas temperature. Therefore the pressure was manually controlled and constrained between 50 to 150 $mbar$; it has been ascertained that, when the pressure exceed $200 - 220\,mbar$, the convective fluxes are predominant over the radiative ones and the temperature of the radiator plates, in the third state, rapidly evens out. Further studies on the thermal properties of the air at low pressure are needed, but it is not the

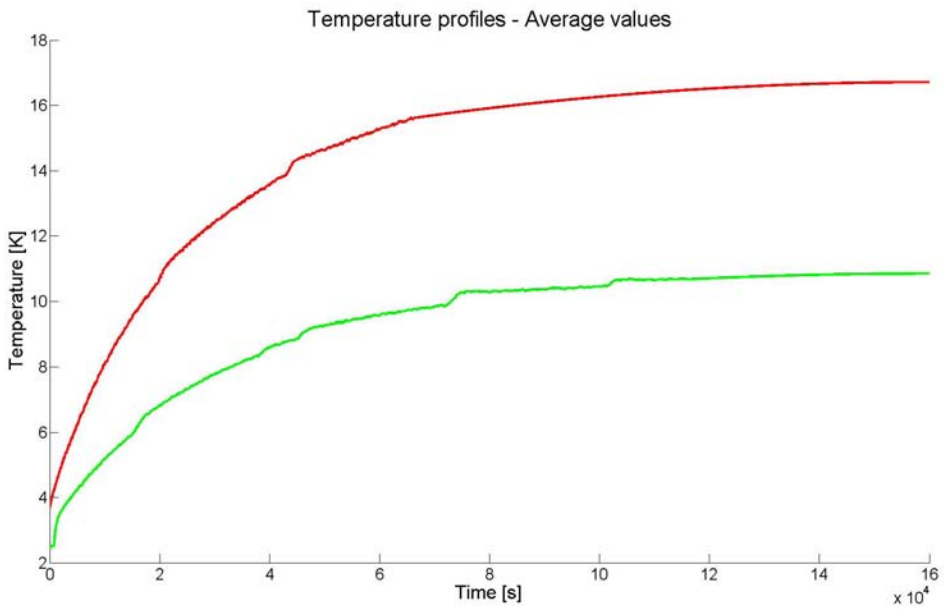

Figure 3.7: Average temperature values

subject of this essay [4]. The temperature never reaches a stationary value: this is due to the conductivity of the structure. Indeed, even if the experiment was built in order to minimize the parasitic heat transfers, few remains (it is impossible to reach an infinite resistance).

The maximum temperature difference within a single plate sensed by the RTDs occurs on the external plate and the difference is $+3.48\,K$, as it is possible to see in figure 3.8. This means that the temperature on the center of the plate is more than $3\,K$ higher than the one in the corner in certain situation. This happen when the radiator is in state 3 and thus the plates are not in contact. The temperature of the first plate is roughly uniform and the negative values showed in the plot are senseless since the power resistor is approximately in the center and there the maximum temperature is foreseen. By the way the minimum value is $-0.27\,K$ and is lower than the uncertainty

[4] Even the state-of-the-art models used in the simulation to compute the convective heat transfer coefficient revealed to be incorrect in the tested conditions.

of the measuring chain; this difference is so attributed to errors and not to a physical phenomenon.

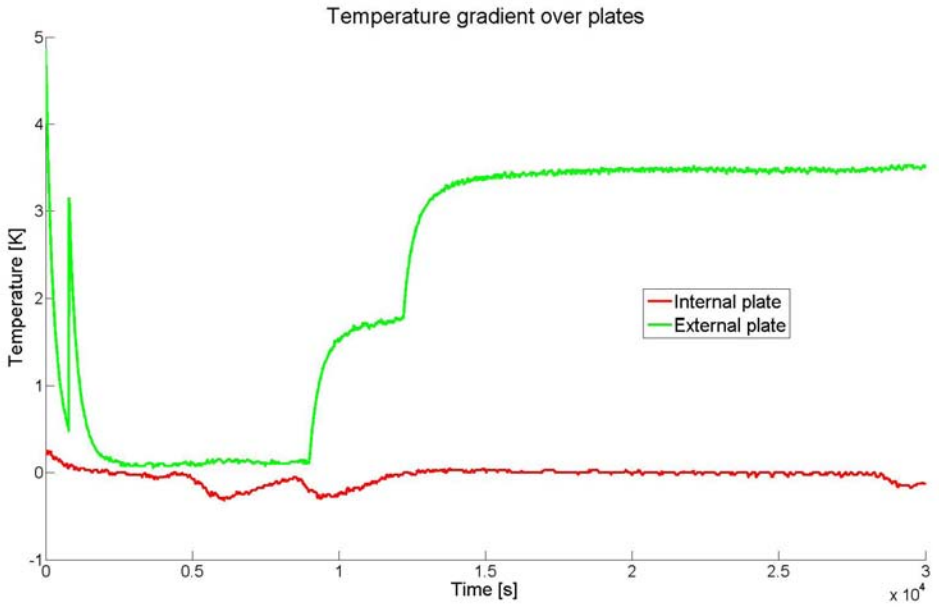

Figure 3.8: Temperature gradient over the radiator plates

The IR radiation affecting the external plate of the radiator remained between 440 to 450 W/m^2. On the other hand the visible radiation never exceeded 2 W/m^2 and thus will be excluded from the calculations. This radiation comes from the little windows on the vacuum chamber, since no other lights were pointed to the experiment during the test campaign.

These data will be later utilized in order to better understand the real potentialities of this concept of heat radiator (in chapter 5).

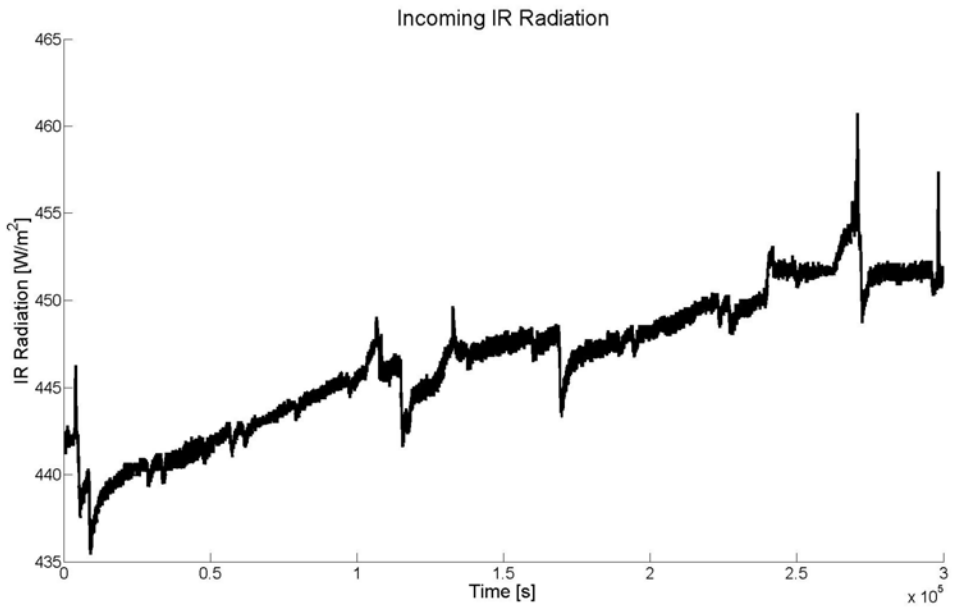

Figure 3.9: Incoming IR radiation

Chapter 4

Stratospheric flight

4.1 Flight data

In this section all the data acquired during a stratospheric flight will be presented. Given flight took place in the BEXUS programme framework.

Figure 4.1: Picture of the POLARIS experiment during the flight

The REXUS/BEXUS programme allows students from universities and higher education colleges across Europe to carry out scientific and techno-

logical experiments on research rockets and balloons. Each year, two rockets and two balloons are launched, carrying up to 20 experiments designed and built by student teams. The programme is realised under a bilateral Agency Agreement between the German Aerospace Center (DLR) and the Swedish National Space Board (SNSB). The Swedish share of the payload has been made available to students from other European countries through a collaboration with the European Space Agency (ESA). Experts from DLR, SSC, ZARM and ESA provide technical support to the student teams throughout the project. REXUS and BEXUS are launched from SSC, Esrange Space Center in Kiruna, northern Sweden.

POLARIS Experiment flew on-board the BEXUS18 Balloon in October 2014.

Some of the following data were provided by the EBASS[11], which is the service unit on the BEXUS balloon. This include pressure and temperature sensors, power delivery control, communication system, GPS receiver etc. It is visible in between the between of the gondola[1] and the balloon itself, just under the parachute.

4.1.1 Pressure and altitude

The first useful information needed to study the behavior of the experiment comes from the pressure sensors. In figure 4.2 it is possible to see the comparison between the POLARIS measured pressure and the one of the EBASS.

As it is possible to see in figure 4.2, the sensors were well calibrated in the CISAS vacuum chamber. POLARIS pressure sensors worked pretty well even in these low pressure environment, where a Pirani[2] is usually preferred

[1] the gondola is the cage under the BEXUS balloon where the experiments are mounted in.

[2] Pirani vacuum gauge is a sensor that measures pressure through thermal conductivity of gas. It is one of the oldest vacuum sensors. The simplest version of the gauge contains a heated plate. The measurement is done by detecting the amount of heat loss from the plate that depends on the gas pressure.

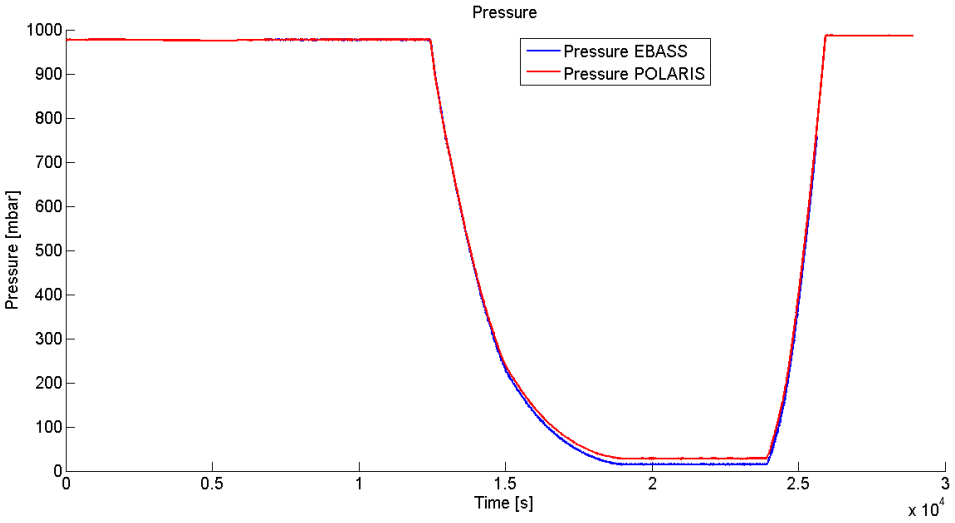

Figure 4.2: Pressure during the flight

to a piezoresistive one. The accuracy of the ADC is far lower than the sensor accuracy, while larger differences are due to a wrong calibration. These data have been used to estimate the altitude with the US Standard Atmosphere model[10]. No other sensors (i.e. GPS) were used to estimate the right altitude because it wasn't a strictly requirement: the main purpose was to inform the software of the beginning of the floating phase in order to start the phases even if all the communications were compromised.

The floating altitude reached was 27300 m (as shown in the GPS data provided by the EBASS in figure 4.3), whit a mean environment pressure lower than 20 mbar, well enough to simulate a possible environment for the POLARIS radiator in future applications. The main objective was to avoid a relevant contribution of the convective heat exchange and from this viewpoint it has been a success.

4.1.2 Environment temperatures

The environment temperature profile encountered during the whole mission was similar to the one predicted and the experiment proved to be well de-

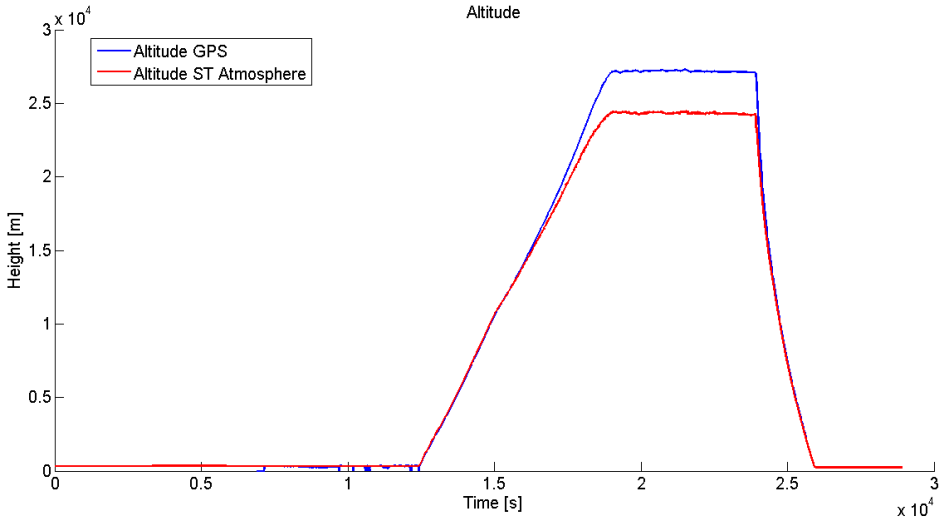

Figure 4.3: Altitude during the flight

signed to use few (if none at all) power to heat itself during the floating phase. The external temperature was measured with a Pt100 class B probe located in the front face of the experiment. It was known that this probe was in contact with the carbon fibre panel, influencing the temperature reading: in fact, as the sun light hit this surface, it raise the surface temperature and the probe measurement was so influenced. By the way, instead of change the design of the experiment setup in order to get a more accurate value of the outer temperature, it was decided to rely on the given EBASS temperature in order to make further calculations. As it is possible to see in figure 4.4 the lowest temperature reached during the flight was 215.5 K ($-57.6°C$).

During the whole flight the internal temperature remained within the required values and for most of the mission time the internal heaters remained turned off. In fact, the software turned them on only on the launch pad in order to be prepared to face the most extreme condition; by the way, during the flight, the insulating composite panels and the heat wasted from the internal electronics were just enough to maintain the temperature inside the experiment between 284 and 293 K. This guaranteed that every subsystem

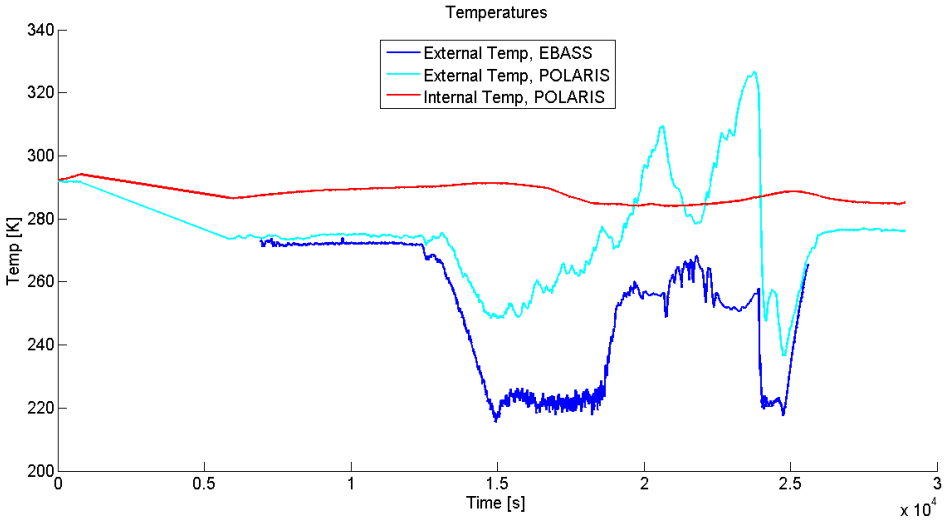

Figure 4.4: Ambient temperature during the flight

worked within the recommended temperature range.

4.1.3 Incoming Radiation

Within the front face of the experiment two radiometers were provided, as described in section 3.1. The first one is a pyranometer (DeltaOhm LP Pyra03) and is mounted to measure the incoming visible radiation, while the other one is a pirgeometer (DeltaOhm LP Pirg01), the most reliable sensor to measure the incoming IR radiation. Both the instruments were previously calibrated and compensated in temperature. The exact value of the incoming radiation is in fact crucial to estimate the correct heat fluxes on the radiator plates: those two radiometers are capable of guarantee measurements with an accuracy of $\pm 2\%$ for a given FOV of $2\pi\ sr$.

Moreover, in figure 4.6, it is possible to see how the presence of the atmosphere and the surrounding objects influenced the IR radiation readout. In fact, when the gondola was on the ground the incoming IR radiation measured was $\sim 300\,W/m^2$, while in floating was as low as $170 - 200\,W/m^2$.

Finally, another important value that we can extrapolate from these sen-

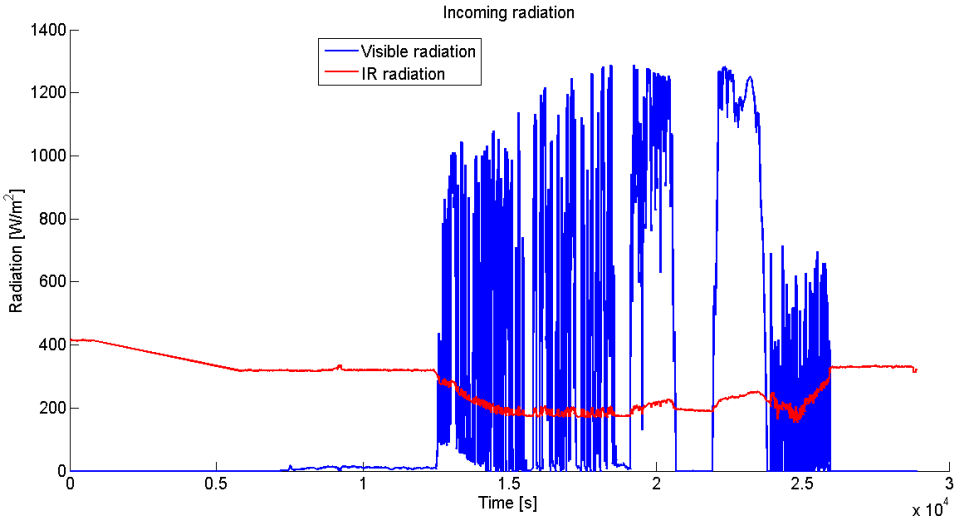

Figure 4.5: Incoming visible and IR radiation during the flight

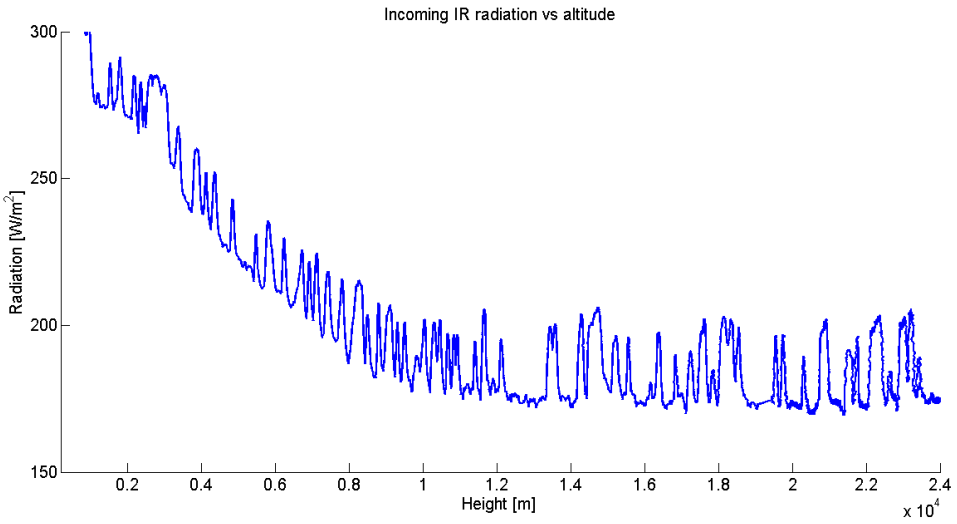

Figure 4.6: Incoming visible radiation during the ascending phase

sors is the period of the gondola rotation. In order to do so the data were windowed, as shown in figure 4.7. This has been done in order to distinguish the two most valuable parts: the first window, in blue, represents the ascending phase, while the red one comprehends the floating phase. The green window has been considered in order to have another detailed esteem of the

rotation frequencies.

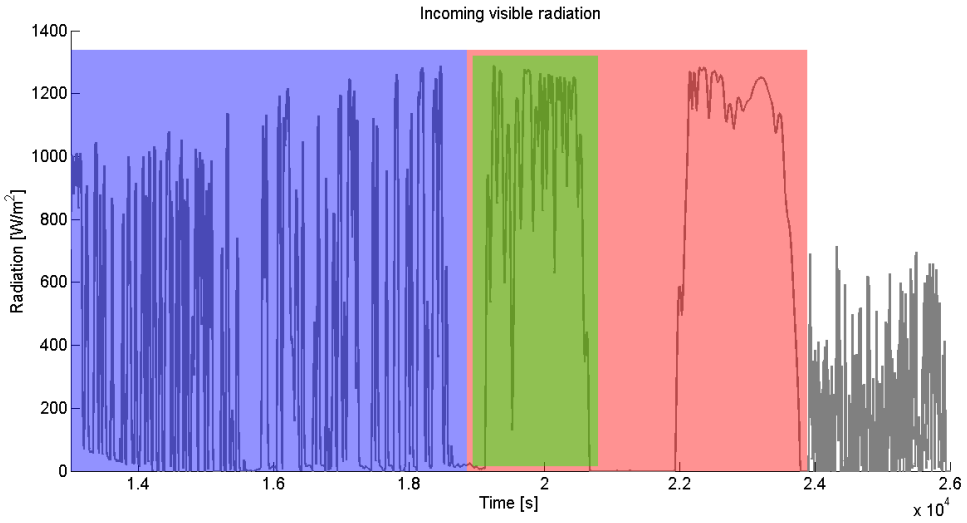

Figure 4.7: Windows used for the FFT

During both the ascending and floating phase of the mission the system disclosed a first clear oscillation at $9.9 \cdot 10^{-4}\ Hz$, which was the BEXUS rotating period of 16 minutes and 50 seconds. This is visible in figure 4.8 and was one of the unpredicted conditions that aroused to the high temperatures registered on the external plate. No other significant periods were found, except for the 1 minute and 46 seconds ($9.4 \cdot 10^{-3}\ Hz$) in the green window. This means that all the other fluctuation were mostly random and caused by other pitch and yaw rotations of the gondola respect to the sun.

However, the floating phase is far more stable than the ascending one as can be seen in figure 4.8, where the floating phase is represented by the red line while the blue line, the one extrapolated during ascending, shows more noise. The most important data were recorded during the red (floating) phase: here the experiment had about 25 minutes of constant light and 21 minutes of darkness.

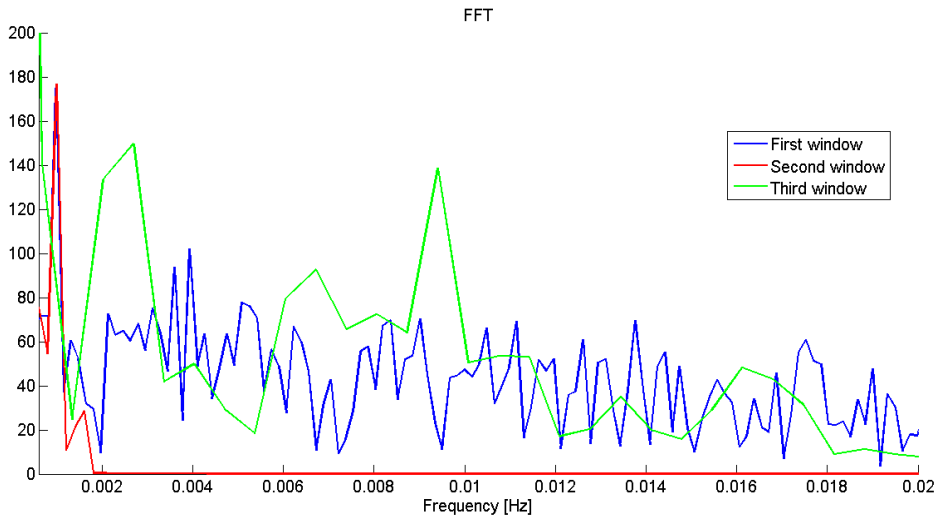

Figure 4.8: FFT results

4.2 Experiment behavior in stratosphere

The duration of the BEXUS18 flight has been considerably shorter than the optimal flight time requested for the experiment. Thus, it is difficult to evaluate the POLARIS radiator performances directly from the flight data. A qualitative value of the radiator performances is the ratio R between the equivalent thermal resistance of the radiator in its two configurations (separated plates and tightened plates). The equivalent thermal resistance of the two configurations has been estimated approximating the transient behaviour of the temperature difference between the internal and the external plates with an exponential equation as shown in 4.1

$$T_t = T_0 + \Delta T \cdot (1 - e^{-t/\tau}) \tag{4.1}$$

Where T_t represents the temperature difference at time t, T_0 represents the temperature difference before the actuation, ΔT represents the temperature difference between the two radiator configurations and τ represents the characteristic constant of the process. The characteristic constant is pro-

portional to the product of thermal resistance and the thermal capacity of the system. Since the thermal capacity of system is the same in the two configurations, the ratio R between the equivalent thermal resistances can be computed also as the ratio between the characteristic constants of the opening and closing processes of the radiator plates.

$$R = \frac{R_{eq}^{separated}}{R_{eq}^{tightened}} = \frac{\tau^{opening}}{\tau^{closing}} \tag{4.2}$$

The procedure shown in equation 4.2 has been applied with the most favourable data gathered during the flight, while the experiment was not pointing towards the sun and all the incoming thermal fluxes were approximately constant. In this situation the estimated ratio R assumed a value between 1.88 and 2.03. Due to the unexpected environmental conditions encountered during the flight and the short mission duration, it has been difficult to estimate quantitatively the performances of the POLARIS radiator, especially in terms of the ratio between the different equivalent thermal resistances of the radiator configurations.

It is possible to give a qualitative analysis of the radiator performances and the figure 4.9 is particularly helpful regarding this topic. The graph shows the real temperature of the dummy payload connected to the radiator together with the estimated temperature of the dummy payload connected to a standard single plate radiator (same material and emissivity of the last plate of POLARIS), in a particular moment of the flight. In order to present a more complete set of information about the radiator, other parameters were added to the diagram: on one hand, the environmental conditions are considered highlighting sunlight exposure and shadow with different colors (respectively yellow and blue); on the other hand, the open/closed configurations are showed using a black line (low is state 1 with closed plates, high is state 3 with open plates).

Considering the different parts of figure 4.9, it shows that POLARIS worked as expected:

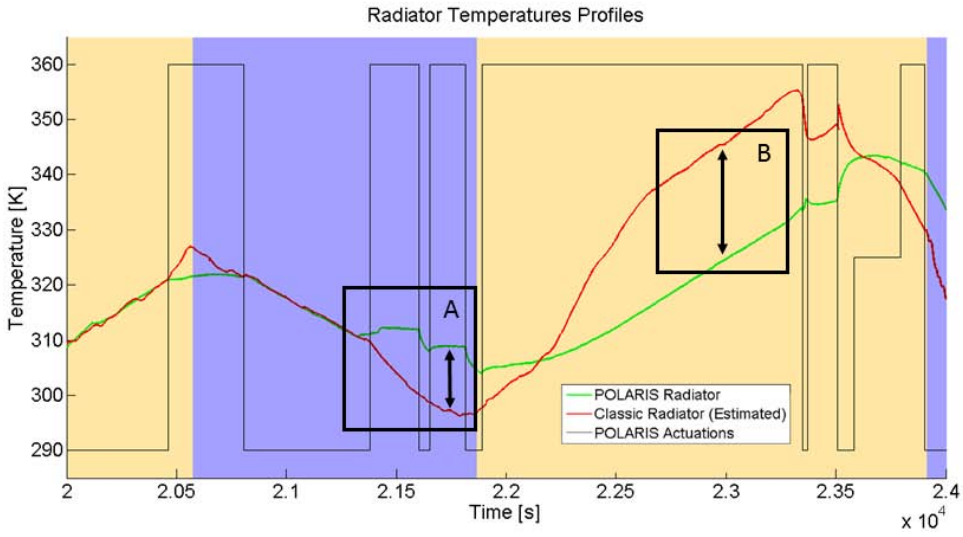

Figure 4.9: POLARIS vs a classic radiator

Left part (before $2.05 \cdot 10^4 s$) Sunlight Exposure, the three plates are initially in contact. It is evident that the two radiators create the same effect on the payload temperature; this is an important result, because it shows how the three plates in contact could be assimilated to a single plate.

Rectangle A Shadow Exposure and consequent cold conditions, the three plates were opened two times. It is evident how the opening of the plates strongly increases the payload temperature in respect with the standard radiator.

Rectancle B Sunlight Exposure and consequent hot conditions, the three plates are opened. It is evident how the opening of the plates strongly

insulates the payload in respect with the standard radiator.

In conclusion, the flight conditions were not the best to perform a quantitative test on the radiator performance, but they were a great test bench for the whole system because of the extreme different conditions faced by the experiment. This encouraging results confirm that the radiator does exactly what it was designed for.

Chapter 5

Performance Analysis

In section 3.1 a hint of the radiator performances was given, but in this chapter it will be better examined. It is, however, useful in this context analyze the data collected during the flight before any further considerations on the laboratory tests.

Moreover, it is important to detail how the contact thermal resistance between the radiator plates has been computed. In fact, to ensure a good thermal link between the metallic plates, a thermal pad was applied (for reference the LAIRD Tpli 210 FG A0 thermally conductive gap filler). Some of the most interesting things about this pad are:

- Good thermal conductivity
- Shock and vibration absorber
- Low outgassing
- Wide working temperature

In particular, the thermal impedance as function of the contact pressure and the values are stated by the manufactured. A great characteristic of this thermal pad is that it shows only a little resistance difference due to the contact pressure, permitting to work with forces much smaller than those

required by a purely metallic contact. The only force that keeped the plates together during all these tests was a Firgelli L12 linear actuator that pulls the external plate toward the internal one, trailing accordingly the plate in between. This actuator is capable to apply to the radiator 45 N so, since the contact area between the plates and the thermal pads is 0.04 m^2, the pressure in between in 1125 Pa. This is much lower than the optimal pressure required by such devices (stated at around 100 kPa), but enough to guarantee a thermal conductivity of 6 $^{W}/_{m \cdot K}$

5.1 Flight analysis

> When you fly a balloon you don't file a flight plan; you go where the wind goes. You feel like part of the air. You almost feel like part of eternity, and you just float along.
>
> Jeannette Piccard

It is difficult to perform a good characterization of the radiator from given data, since the conditions faced by the experiment during the flight were very variable and the experiment did not have enough time to coll down to a steady temperature. Only a precise time span, at about two hours and a half after takeoff, was ideal to the experiment, and it is the one showed in figure 5.1. Please note that in this figure the temperatures are normalized as described in section 3.2.

The experiment was in stratosphere at an altitude of 27.2 km and the ambient pressure was 15 $mbar$. During this time the experiment was not facing the Sun (it seems that neither the albedo was perceivable, thus the visible radiation incoming was $\sim 0\ W/m^2$), the IR incoming radiation had a steady value of $G_{IR} = 192\ W/m^2$ and the external temperature was stationary at

265 K. The measured heat fluxes that directly conditioned the radiator are illustrated in figure 5.2. Only one of the three power resistors was turned on and the power dissipated towards the radiator was 7.4 W. Since the resistance of the power resistor is 100 Ω and it is directly connected to the BEXUS batteries, it is possible to calculate the voltage drop of the batteries with equation 5.1, where P is the power dissipated and R is the resistance value. V_{drop} is the voltage drop in the power MOSFET that control each resistor, and it is stated at 0.8 V.

$$V = \sqrt{P \cdot R} + V_{drop} \tag{5.1}$$

It is, therefore, easy to calculate that the voltage supplied by the batteries was perfectly 28 V, as guaranteed by the SSC staff. This assured that every electronic subsystem worked as designed.

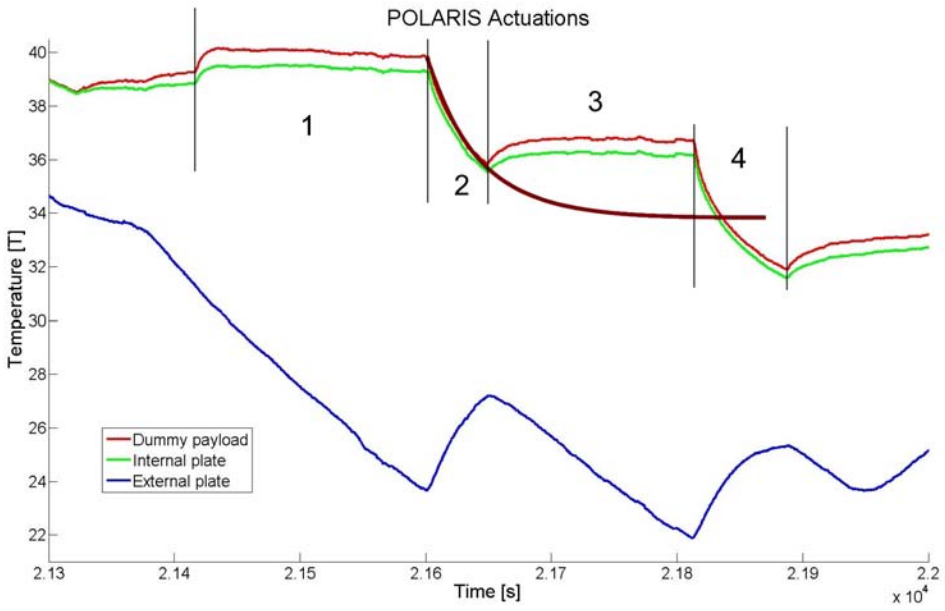

Figure 5.1: POLARIS actuations during the stratospheric flight

Since the external plate of the radiator have an active area of 20×20 cm

($0.04\ m^2$) and a absorption coefficient $\varepsilon = 0.975$[1] the total heat exchanged is described in equations 5.2 and 5.3, where G_{IR} is the IR radiative specific flux and the other variables have been introduced yet. The convective heat flux was negligible, for a more accurate explanation please refer to the SED[13].

$$q = [\sigma \cdot \varepsilon \cdot A \cdot T^4_{external\ plate}] - [A \cdot \varepsilon \cdot G_{IR}] \tag{5.2}$$

$$q = 2.211 \times 10^9 \cdot T^4_{external\ plate} - 7.488\ [W] \tag{5.3}$$

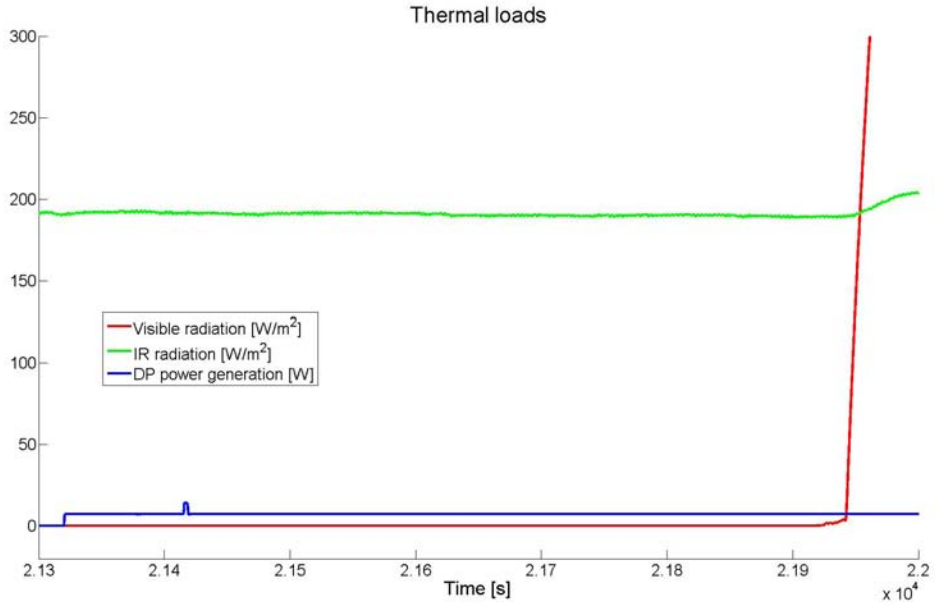

Figure 5.2: Direct heat fluxes applied to the radiator

It is now possible to divide in 4 different sections this time window, as is visually noticeable in figure 5.1 where the ~ 10 minutes window is focused.

Section 1 During this phase the radiator was in state 3 (so the plates were separated one from each other) and it is evident how the radiator was

[1]The coating applied on the external plate of the radiator is a NEXTEL® Velvet Coating 811-21 by Mankiewicz. It has a stable emissivity over a wide temperature range [9].

able to isolate the payload from the outer environment. In fact, while the DP temperature decreased by only 0.6 K, the external plate temperature dropped 6.8 K in three minutes. With the equation 2.14 it is possible to evaluate the flux between the plates and it increase from 0.9 to 1.76 W (the evolution in time is shown in figure 5.3). The heat flux within the radiator almost doubled in only three minutes; by the way it is possible to calculate the equivalent thermal resistance R_{open} according to equation 5.4 (passages are those described for equation 2.16). In this window the average radiator temperature is 281.87K and the emissivity of the plates is set to 0.2[2].

$$R_{open} = \frac{{}^{1}/_{\varepsilon_1} + {}^{1}/_{\varepsilon_2} - 1}{4 \cdot \sigma \cdot T_m^3} \tag{5.4}$$

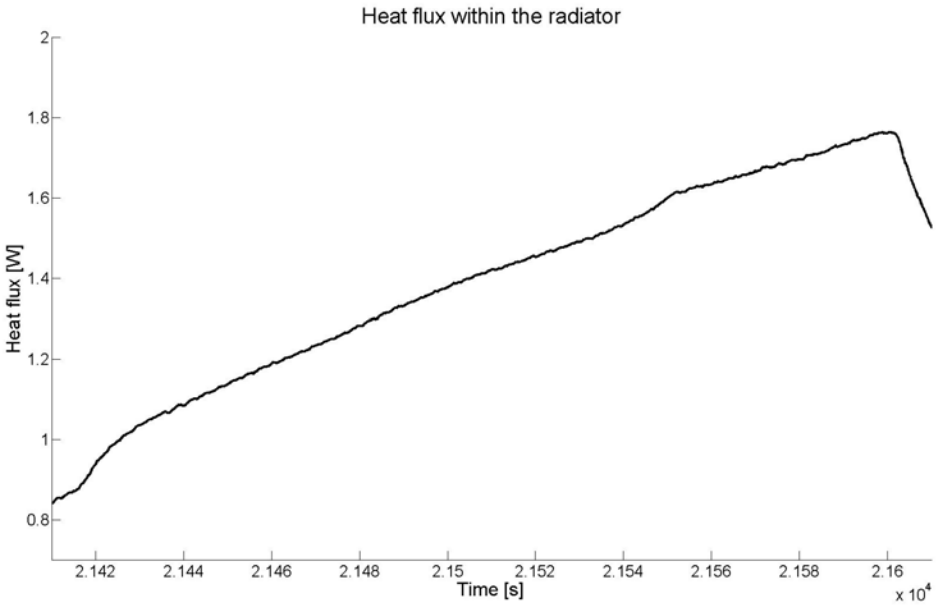

Figure 5.3: Heat flux within the radiator

[2]The emissivity ε of a bare aluminum plate is slightly lower than this value, but, since the thermal pad (a Laird Technologies Tpli^{TM}) 210 has a stated emissivity of 0.22, an average value has been used[13]

Thus, the computed specific thermal resistance factor is 1.77 $^{m^2 \cdot K}/_{W}$. Therefore POLARIS was able to isolate the DP from the environment, dissipating less than 2 W in view of the 7.4 W produced. Since the heat dissipated through the plates was much lower than the heat produced by the DP and its temperature was not increasing, it is evident that other thermal paths were established. This phenomena is more evident in the stratospheric flight, respect to the laboratory test in section 3.2, since the temperature difference between the radiator and the ambient and, thus, the structure, is higher. In fact, while in the laboratory the DP temperature was only $\sim$ 10 to 15 K higher than the surroundings, during the flight the difference reached a $\Delta T = 40$ K, making relevant the parasitic heat fluxes

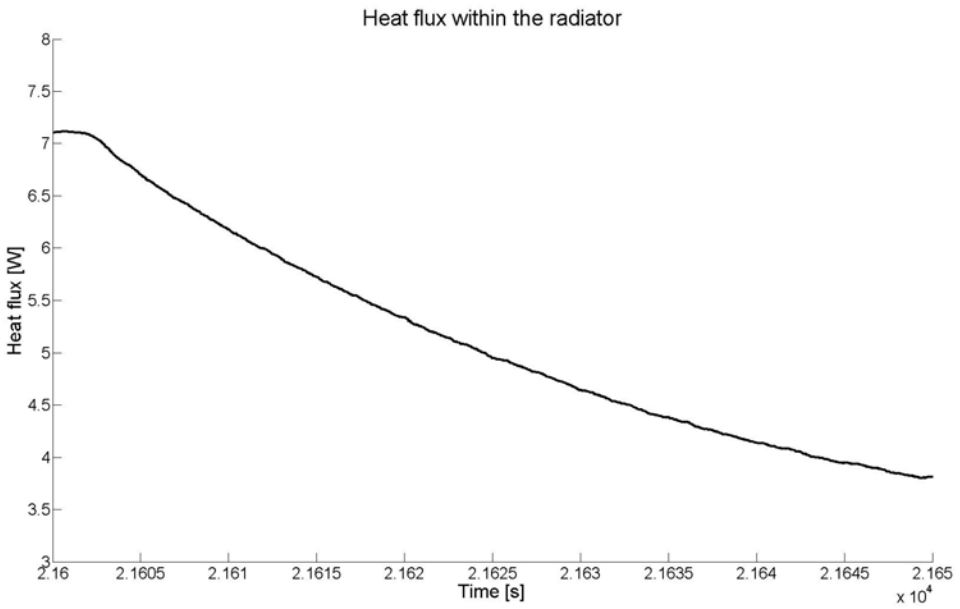

Figure 5.4: Heat flux within the radiator

Section 2 The radiator here switched to state 1 and, as soon as the plates got in contact, temperatures began to mediate. The DP rapidly cooled down and the thermal resistance, now calculated with equation 2.12, is

$0.88\ {}^{m^2 \cdot K}/_{W}$, which is halved respect to the previous state. In figure 5.1 it is illustrated, with a darker red line, the simulated behavior of the radiator if it had enough time to reach a stable temperature. The curve is a fit of the measured evolution, made accordingly to an exponential trend, similar to an electrical RC discharge circuit 5.5.

$$V(t) = V_0 \cdot e^{-{}^{t}/_{RC}} \tag{5.5}$$

The *steady state* temperature difference between this and the first section is 5 K and it compatible with the data shown in figure 3.6. However this is a totally different situation since the starting temperatures of the three plates were very different and further comparisons would be useless. In less than 50 s the DP temperature decreased of $4K$ while the third plate gained 3.5 K. The heat exchanged between the plates is showed in figure 5.4, and it is applicable the same consideration made for the parasitic heat fluxes in section 1.

Section 3 The radiator separated one more time the plates and the DP stabilized again its temperature. Even if the radiator was designed to *increase* the DP temperature and not to *stabilize* it, the boundary conditions were not favorable to this to happen. With hindsight two design drivers were to change: the power dissipated by the DP could have been higher (and it was possible simply by turning on another power resistor, but it was too risky for the mission to change a main factor during the flight) or, better, the active area of the radiator could have been smaller. It is interesting to notice that, while it takes more than two minutes for the state 1 to become stable, it only takes $20-30s$ for the state 3 (this is mainly caused by the thermal capacity of the plates).

Section 4 This is the last useful time window before the sunlit period, where the incoming visible radiation was overwhelming respect to the other

fluxes (the higher specific flux reached 1288 W/m^2); in fact, in figure 5.2, it is possible to notice on the right side of the diagram that the incoming visible started to increase. All the considerations made for *section 2* are here validated.

At the conclusion of this analysis the most important thing to highlight is the ability of the radiator to double its resistance when needed, even if the boundary conditions were not ideal to the test. During the flight much more have been tested, but it is not pertinent to this essay. A longer flight may have helped, together with a better design in order to avoid parasitic heat fluxes. In fact, balancing the fluxes at the beginning of *section 1* it is possible to realize that a lot of heat is wasted through the structure of the experiment setup. In equation 5.6 is computed the heat flux $q_{internal\ plate}$ that reach the first plate and, with few algebraic, it is $q = 7.4 - 0.9 = 6.5\ W$. Since the temperature of the first plate did not show a remarkable increase in its temperature, it is assumed that all of this heat is dissipated through the structure.

$$q_{internal\ plate} = q_{DP} - \frac{4 \cdot A_{plate} \cdot \sigma \cdot (T^4_{internal\ plate} - T^4_{external\ plate})}{{}^{2}/_{\varepsilon} - 1} \tag{5.6}$$

This occurrence is unsatisfactory to the data analysis, but improves in the test campaign results described from now on.

5.2 Test analysis

In order to avoid the issues faced during the flight in stratosphere mentioned above, during the test in the laboratory the radiator temperature was maintained as near as possible to the ambient one. So, only a single power resistor (which was dissipating 8.97 W) was turned on and all the external fluxes that reach the external plate were avoided when possible. Inside the vacuum chamber, in fact, there are three LED lamps, which were used in

previous tests, but were turned off during these ones. Thus, only the stable IR radiating flux was conditioning the radiator, which average specific value was 445 W/m^2, that correspond to a net flux of 17.36 W on the external plate.

In figure 3.7 the average pace of the DP temperature have been described, but now it is useful to add also the average external plate temperature as depicted in figure 5.5. This is essential to calculate the heat flux exchanged within the radiator plates.

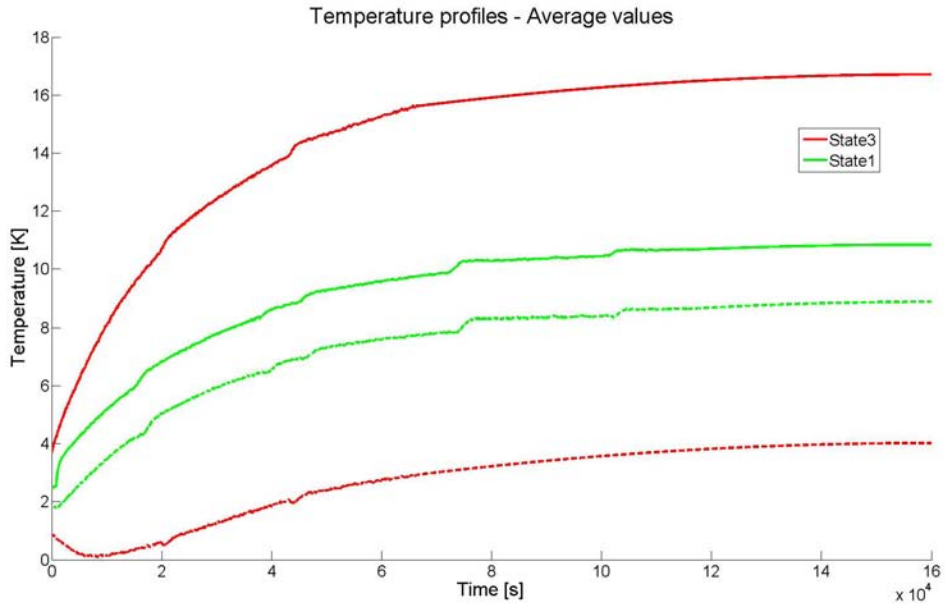

Figure 5.5: Average DP and external plate temperature values

The recorded data of the two different states are shown in figure 5.5, in which the solid line represents the DP temperature and the dotted one represents the external plate one. It is immediately noticeable that the temperature gap is much bigger while in state 3, as predicted. In particular, while in state 1 the temperature gap is 1.9 K, in state 3 it is 12.7 K: this is due to the different thermal resistance of the POLARIS radiator and will be here quantified.

The thermal resistance in the closed plates condition is the one already described in section 5.1,: since that the only factors that influence it are those inherent to the radiator itself, it does not change between the various test campaigns. Hence, since no changes have been made to the radiator between the flight and the laboratory tests, the reference value for the thermal resistance is still 0.88 $^{m^2 \cdot K}/_{W}$. Computing all the heat fluxes from the given data at the *steady state* condition disclose that $\sim 2\ W$ are wasted through the structure, which is a third than the value dissipated during the flight. The thermal resistance in state 3 is 1.34 $^{m^2 \cdot K}/_{W}$, computed with equation 5.4. It is lower than the one calculated with the flight data, since the average temperature of the radiator is higher, facilitating the radiative heat flux between the radiator plates. By the way, this value can dramatically change in other environment: in example, a similar radiator mounted on an atmospheric probe flying on Mars, should be able to show a resistance in state 3 as high as $2.5 - 3$ $^{m^2 \cdot K}/_{W}$. This is due to the low ambient temperature and is function of the mean temperature of the radiator, so also the required temperature for the payload is a driving factor for the calculations.

The switch between state 1 and state 3 increase the DP temperature of 5.9 K, which is a +54% increase in temperature - a lot considering that the radiator is overstated for such a heat load. In other words it is able to precisely control (via a PWPFM software) the DP temperature in a 6 K range.

Another important fact to consider is that the time required by the DP to cool down is much shorter than the one required to heat up. Thanks to the good heat capacity of the aluminum plates it only takes two minutes to drop the temperature from 16.7 to 10.8 K (above ambient temperature). In figure 5.6 it is better displayed how the radiator, switching from state 3 to state 2 and than to state 1, was able to rapidly decrease the temperature of the DP during a test in the vaacuum chamber.

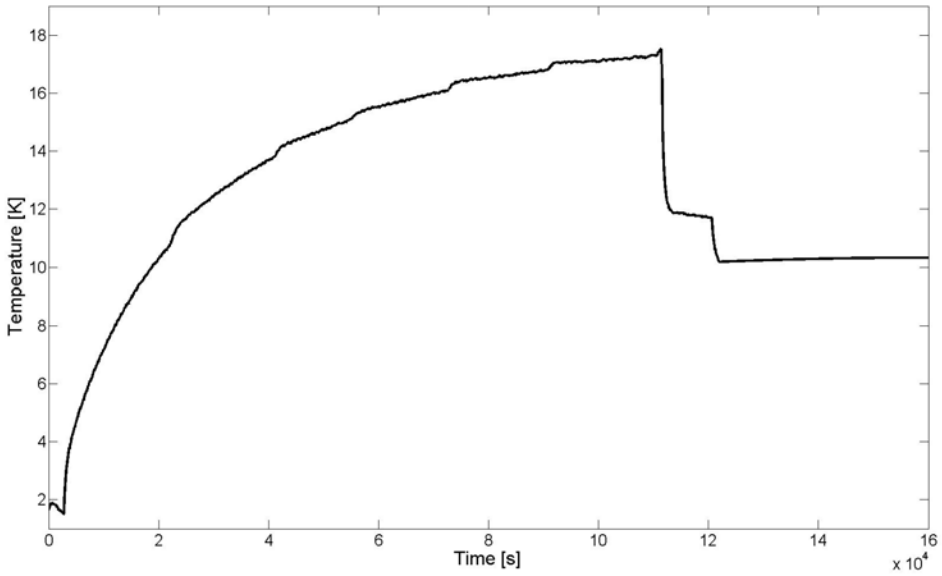

Figure 5.6: Average DP and external plate temperature values

5.3 Performance of the setup

POLARIS radiator was designed to increase its resistance three times during a stratospheric flight, by the way it only managed to doubled it since the short flight time did not allow to reach a steady low temperature and the incoming visible radiation was so strong that the external plate reached a very high temperature (over 360 K) in certain moments, making such recorded data useless to a performance analysis. By the way, as described in figure 4.9, it managed to mitigate the temperature of the DP during the most hostile phases of the mission.

The laboratory test revealed its ability increase or decrease the DP in matter of minutes. The average rates are $-0.5\ K/min$ and $+0.1\ K/min$ in a range of 6 K. During these tests the ambient temperature was as high as 299 K and, thus, the resistance computed in state 3 was only 50% greater than the one in state 1, but in different environments the situation could change dramatically. Many simulations have been carried out with the mea-

sured data and show that, with a new experiment setup, performances could be much higher[3]. The net heat radiated from the external plate varied from 1.2 to 2.5 W (measured at the equilibrium conditions) as shown in figure 5.7, so the setup was able to double the heat dissipated from state 3 to state 1.

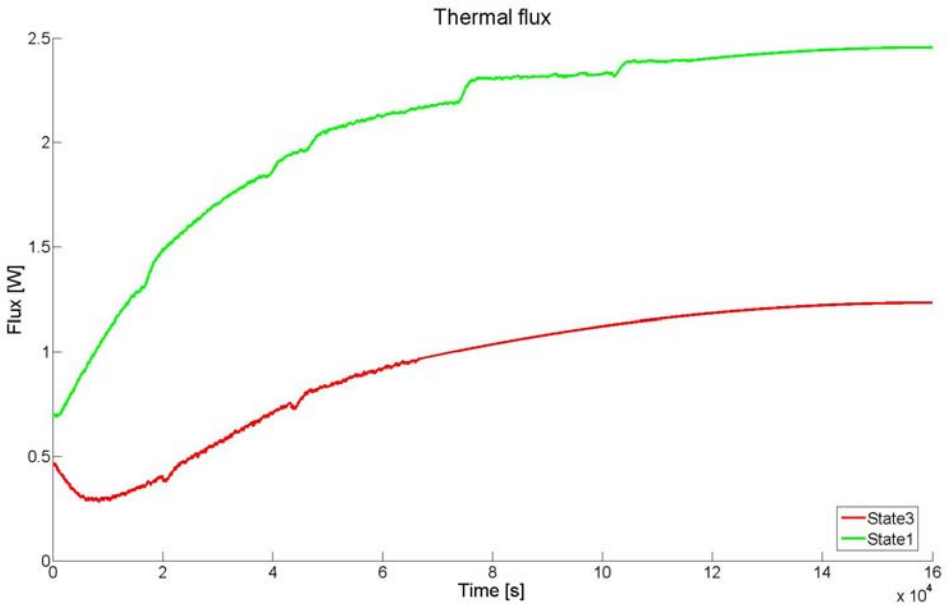

Figure 5.7: The net radiative flux exchanged between the external plate and the environment

In figure 5.8 it is possible to have a better view of the POLARIS front face, displaying the external radiator plate and the RTDs mounted over it. In this experiment setup many design drivers could have been changed, among others:

- Increase the number of plates in order to raise the radiator thermal resistance in state 3. Its behavior is similar to the one described for the MLI blankets in figure 1.4

[3]Some information on these simulations is present in the SED[13], but additional work is in the plans.

- Decrease the thickness of the plates in order to reduce the resistance in state 1 and, if possible, avoid the use of the thermal pad in between. This involve a more advanced plates manufacturing because both the flatness and the roughness of the plates must respect tighten values
- Optimize the design of the experiment setup in order to avoid as much as possible parasitic thermal paths

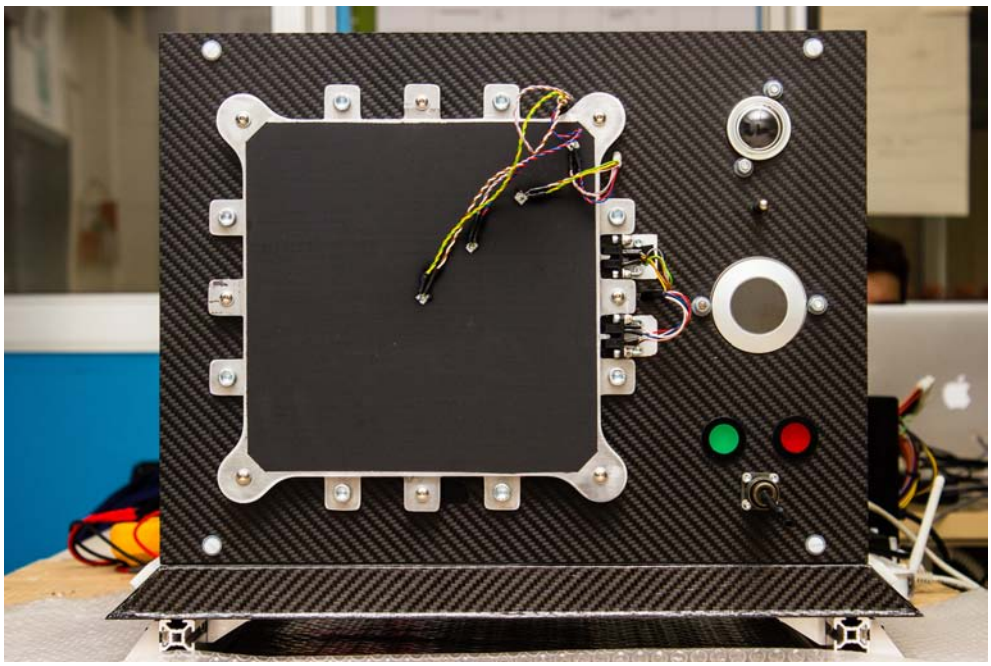

Figure 5.8: Picture of the experiment setup

In conclusion, results showed that every temperature between the two equilibrium values above is achievable and maintainable within a small tolerance range. This is easily achievable with a few power consumption and by command of a simple and reliable algorithm. This outstanding feature indicates that the most likable scenario for this device is the one with satellites that strongly need active thermal control, such as satellites subjected to extreme, hardly predictable random variation of the environmental thermal loads or other stratospheric probes.

Chapter 6

Conclusions

> Hofstadter's Law: It always
> takes longer than you expect,
> even when you take into account
> Hofstadter's Law.
>
> Douglas Hofstadter

In the previous chapter the principle behind a multi-plate radiator have been explained and the performances of the POLARIS experiment setup described. A direct comparison with other radiators is very difficult to carry out since every space mission has its own specific requirements and thus the TCS is adequately designed. by the way some considerations can be made.

The most advanced kind of radiators are those that involve louvers, which can vary the radiating power by meaning of a change in the emissivity properties. By the way they are usually spring-controlled and the switch temperature is decided in the design phase of the mission. As described in section 1.4, a state of the art louver radiator is capable of increase six times the heat exchanged with the environment, while the first prototype of this multi-plate was capable to double it: this is a very promising factor for future developments. This is a very Thus, if in a certain mission phase the requirements changes, there is nothing that the spacecraft can do. Moreover, the low

emissivity coatings degrade much more rapidly than the high one, making the radiators that do not involve those more durable. POLARIS on the other hand expose to the environment only a high emittance plate and could be controlled by the software to work in a high temperature range. However it is not easy to compare the resistances described in the previous chapters because this radiator can change the heat dissipated by mean of a change in the temperature of the external plate and not by a change in the thermo-optics characteristic of the plate itself.

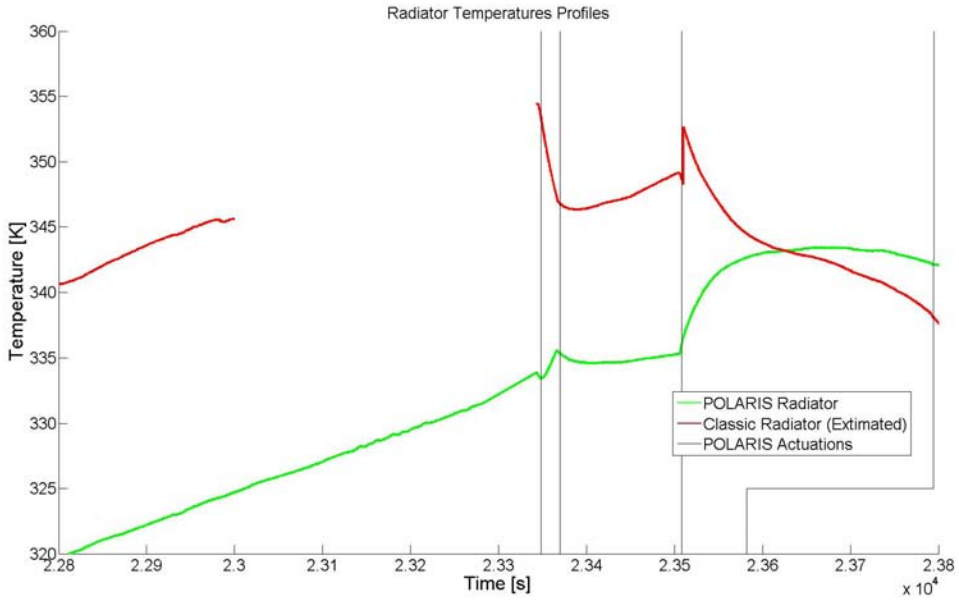

Figure 6.1: Detail of the different behavior between POLARIS and a standard radiator

It is also important to recall another characteristic that distinguish POLARIS from the other radiators. In fact, it was able to isolate the DP during the stratospheric flight throughout the sunlit phases. By better analyzing figure 4.9 (a detail is showed in figure 6.1) it is possible to see that[1], even if the temperature absolute values were very high, the flying setup was able to

[1]The lack of data in figure is due to a software reboot that happened during the flight

mitigate the temperature of more than 20 K in respect to a classic radiator composed only by a high emittance plate. This means that, with an appropriate design, this radiator is able to guarantee the survival of the spacecraft's instruments even in the worst hot-case scenario. These situations could be during a failure of the ADCS or in missions that have to travel both very close and very far to a star.

I would like to thank all the people who contributed to the success of the POLARIS experiment. First of all to the POLARIS team, that participated in the REXUS/BEXUS programme and together built the experiment setup. We started as colleagues to become friends. I am grateful for the assistance given by Prof Alessandro Francesconi and by Francesco Branz, Lorenzo Olivieri and Francesco Sansone during the development of the experiment.

In picture 6.2 from left to right: Tommaso Cortese, Matteo Lora, Marco La Grassa, Matteo Zorzan, Federico Cipriani, Davide Paganini, Cristian Cacco, Francesco Cocco, Riccardo Dalla Vecchia

Figure 6.2: The POLARIS team

Bibliography

[1] Alberto Cavallini and Lino Mattarolo. *Termodinamica Applicata (Applied Thermodynamic)*. Cleup Editore, 1992.

[2] Requirements ECSS Secretariat, ESA-ESTEC and Standards Division. *Space Engineering - Space Environment (ECSS-E-ST-10-04C)*. European Cooperation for Space Standardization, November, 2008.

[3] International Organization for Standardization. Iso 2533:1975, 1975.

[4] Jacob Fraden. *Handbook of Modern Sensors. Physics, Designs, and Applications*. Springer, 2010.

[5] David G. Gilmore. *Satellite Thermal Control Handbook*. The Aerospace Corporation Press, 1994.

[6] John R. Howell. *Thermal Radiation Heat Transfer, 5th Edition*. CRC Press, 2010.

[7] ASTM International. *Standard Tables for Reference Solar Spectral Irradiances (ASTM G173 - 03)*. 2012.

[8] NASA JHUAPL. MESSENGER NASA mission to mercury launch press kit, 2007.

[9] Eric Tang Kwor and Simone Mattel. *Emissivity measurements for Nextel Velvet Coating 811-21 between* $-36^{circ}C$ *and* $82^{circ}C$. Laboratoire d'Energetique et de Thermique Industrielle de l'Est Francilien, 1999.

[10] United States Committee on Extension to the Standard Atmosphere (COESA). *U.S. Standard Atmosphere*. National Technical Information Office, Springfield, Virginia, 1976.

[11] REXUS/BEXUS Organizers. *BEXUS user manual*. EuroLaunch, February, 2014.

[12] Graham Swinerd Peter Fortescue, John Stark. *Spacecraft Systems Engineering*. John Wiley & Sons Ltd, 2003.

[13] POLARIS Team. POLARIS student experiment documentation, 2014.

Glossary

ADC Analog to Digital Converter. 42

ADCS Attitude Determination and Control System. 68

BEXUS Balloon EXperiments for University Students. vii, ix, 20, 25, 27, 41, 42, 47, 54

CF Configuration Factor. 24, 25

CISAS Center of Studies and Activities for Space. vii, 29, 42

DE Dielectric Elastomer. 16, 17, 18

DLR Deutsches Zentrum für Luft- und Raumfahrt. ix, 41

DP Dummy Payload, a heat source placed in order to simulate the heat produces by a real payload. vii, viii, 16, 18, 19, 25, 26, 33, 34, 35, 36, 56, 57, 58, 59, 61, 62, 63, 68

EBASS Esrange Balloon Service System. 42, 43

ESA European Space Agency. vii, ix, 5, 12, 41

FFT Fast Fourier Transform. viii, 46, 47

FOV Field Of View. 45

GPS Global Positioning System. 42, 43

GUI Graphical User Interface. viii, 34

IR Infra Red. viii, 1, 2, 3, 4, 5, 6, 19, 32, 39, 45, 54, 55, 60

LEO Low Earth Orbit. 1

MESSENGER MErcury Surface, Space ENvironment, GEochemistry, and Ranging. vii, 12, 13, 71

MLI Multi Layer Insulator. 9, 64

MOSFET Metal-Oxide-Semiconductor Field-Effect Transistor. 54

MPO Mercury Planetary Orbiter of the BepiColombo mission. 11

MTBF Mean Time Between Failures. 5

NASA National Aeronautics and Space Administration. vii, 1, 12, 13, 71

PCB Printed Circuit Board. 19

PCM Phase-Change Materials. 5, 8

POLARIS POLymer-Actuated Radiator with Independent Surfaces. viii, ix, 15, 18, 19, 20, 22, 23, 29, 32, 34, 41, 42, 43, 47, 49, 55, 57, 61, 63, 64, 67, 68, 70, 72

PWPFM Pulse-Width Pulse-Frequency Modulation. 62

REXUS Rocket EXperiments for University Students. 41

RTD Resistance Temperature Detector. vii, 30, 33, 38, 64

SBC Single Board Computer. 18, 19, 31, 34

SED Student Experiment Documentation. 20, 33, 55, 63

SNSB Swedish National Space Board. ix, 41

SSC Swedish Space Corporation. 55

TCS Thermal Control System. 1, 4, 5, 11, 67

UV Ultraviolet light is electromagnetic radiation with a wavelength from 400 nm to 10 nm. 1